https://doi.org/10.5194/bg-2020-147
Preprint. Discussion started: 14 May 2020

Biogeosciences
Discussions
Open Access
EGU

Implementation of nitrogen cycle in the CLASSIC land model

Ali Asaadi and Vivek. K. Arora

Canadian Centre for Climate Modelling and Analysis, Environment Canada, University of Victoria, Victoria, B.C., V8W 2Y2, Canada

https://doi.org/10.5194/bg-2020-147
Preprint. Discussion started: 14 May 2020

Biogeosciences Discussions

Abstract

A terrestrial nitrogen (N) cycle model is coupled to carbon (C) cycle in the framework of the Canadian Land Surface Scheme Including biogeochemical Cycles (CLASSIC). CLASSIC currently models physical and biogeochemical processes and simulates fluxes of water, energy, and CO_2 at the land-atmosphere boundary. Similar to most models, gross primary productivity in CLASSIC increases in response to increasing atmospheric CO_2 concentration. In the current model version, a downregulation parameterization emulates the effect of nutrient constraints and scales down potential photosynthesis rates, using a globally constant scalar, as a function of increasing CO_2. In the new model when N and C cycles are coupled, cycling of N through the coupled soil-vegetation system facilitates the simulation of leaf N content and maximum carboxylation capacity (V_{cmax}) prognostically. An increase in atmospheric CO_2 decreases leaf N content, and therefore V_{cmax}, allowing the simulation of photosynthesis downregulation as a function of N supply. All primary N cycle processes, that represent the coupled soil-vegetation system, are modelled explicitly. These include biological N fixation, treatment of externally specified N deposition and fertilization application, uptake of N by plants, transfer of N to litter via litterfall, mineralization, immobilization, nitrification, ammonia volatilization, leaching, and the gaseous fluxes of NO, N_2O, and N_2. The interactions between terrestrial C and N cycles are evaluated by perturbing the coupled soil-vegetation system in CLASSIC with one forcing at a time over the 1850-2017 historical period. These forcings include the increase in atmospheric CO_2, change in climate, increase in N deposition, and increasing crop area and fertilizer input, over the historical period. The model response to these forcings is consistent with conceptual understanding of the coupled C and N cycles. The simulated terrestrial carbon sink over the 1959-2017 period, from the simulation with all forcings, is 2.0 Pg C/yr and compares reasonably well with the quasi observation-based estimate from the 2019 Global Carbon Project (2.1 Pg C/yr). The contribution of increasing CO_2, climate change, and N deposition to carbon uptake by land over the historical period (1850-2017) is calculated to be 84%, 2%, and 14%, respectively.

https://doi.org/10.5194/bg-2020-147
Preprint. Discussion started: 14 May 2020

1. Introduction

The uptake of carbon (C) by land and ocean in response to the increase in anthropogenic fossil fuel emissions of CO_2 has served to slow down the growth rate of atmospheric CO_2 since the start of the industrial revolution. At present, about 55% of total carbon emitted into the atmosphere is taken up by land and ocean (Le Quéré et al., 2018; Friedlingstein et al., 2019). It is of great policy, societal, and scientific relevance whether land and ocean will continue to provide this ecosystem service. Over land, the uptake of carbon in response to increasing anthropogenic CO_2 emissions is driven by two primary factors, 1) the CO_2 fertilization of the terrestrial biosphere, and 2) the increase in temperature, both of which are associated with increasing [CO_2]. The CO_2 fertilization effect increases photosynthesis rates for about 80% of the world's C_3 vegetation since photosynthesis for plants that use the C_3 photosynthetic pathway is currently limited by [CO_2] (Still et al., 2003; Zhu et al., 2016). The remaining 20% of vegetation uses the C_4 photosynthetic pathway that is much less sensitive to [CO_2]. Warming increases carbon uptake by vegetation in mid-high latitude regions where growth is currently limited by low temperatures (Zeng et al., 2011).

Even when atmospheric CO_2 is not limiting for photosynthesis, and near surface air temperature is optimal, vegetation cannot photosynthesize at its maximum possible rate if available water and nutrients (most importantly nitrogen (N) and phosphorus (P)) constrain photosynthesis (Vitousek and Howarth, 1991; Reich et al., 2006b). In the absence of water and nutrients, photosynthesis simply cannot occur. N is a major component of chlorophyll (the compound through which plants photosynthesize) and amino acids (that are the building blocks of proteins). The constraint imposed by available water and nutrients implies that the carbon

https://doi.org/10.5194/bg-2020-147
Preprint. Discussion started: 14 May 2020

uptake by land over the historical period in response to increasing [CO_2] is lower than what it would have been if water and nutrients were not limiting. This lower than maximum theoretically possible rate of increase of photosynthesis in response to increasing atmospheric CO_2 is referred to as downregulation (Faria et al., 1996; Sanz-Sáez et al., 2010). Typically, however, the term downregulation of photosynthesis is used only in the context of nutrients and not water. McGuire et al. (1995) define downregulation as a decrease in photosynthetic capacity of plants grown at elevated CO_2 in comparison to plants grown at baseline CO_2, although the rate of photosynthesis for plants grown and measured at elevated CO_2 is still higher than the rate for plants grown and measured at baseline CO_2.

Earth system models (ESMs) that explicitly represent coupling of the global carbon cycle and physical climate system processes are the only tools available at present that, in a physically consistent way, are able to project how land and ocean carbon cycles will respond to future changes in [CO_2]. Such models are routinely compared to one another under the auspices of the Coupled Model Intercomparison Project (CMIP) every 6-7 years. The most recent and sixth phase of CMIP (CMIP6) is currently underway (Eyring et al., 2016). Interactions between carbon cycle and climate in ESMs have been compared under the umbrella of the Coupled Climate-Carbon Cycle Model Intercomparison Project (C^4MIP) (Jones et al., 2016) which is an approved MIP of the CMIP. Comparison of land and ocean carbon uptake in C^4MIP studies (Friedlingstein et al., 2006; Arora et al., 2013, 2019) indicate that the future land carbon uptake across ESMs varies widely and more than three times as much for the ocean carbon uptake. The reason for widely varying estimates of future land carbon uptake across models is that our understanding of biological processes that determine land carbon uptake is much less advanced than the physical

https://doi.org/10.5194/bg-2020-147
Preprint. Discussion started: 14 May 2020

processes which primarily determine carbon uptake over the ocean. In the current generation of terrestrial ecosystem models, other than photosynthesis for which a theoretical framework exists, almost all of the other biological processes are represented on the basis of empirical observations and parameterized in one way or another. In addition, not all models include N and P cycles. In the absence of an explicit representation of nutrient constraints on photosynthesis, land models in ESMs parameterize downregulation of photosynthesis in other ways that reduce the rate of increase of photosynthesis to values below its theoretically maximum possible rate, as [CO_2] increases (e.g. Arora et al., 2009). Comparison of models across 5th and 6th phase of CMIP shows that the fraction of models with land N cycle is increasing (Arora et al., 2013, 2019). The nutrient constraints on photosynthesis are well recognized (Vitousek and Howarth, 1991; Arneth et al., 2010). Terrestrial carbon cycle models neglect of nutrient limitation on photosynthesis has been questioned from an ecological perspective (Reich et al., 2006a) and it has been argued that without nutrients constraints these models will overestimate future land carbon uptake (Hungate et al., 2003). Since in the real world photosynthesis downregulation does indeed occur due to nutrient constraints, it may be argued that more confidence can be placed in future projections of models that explicitly model the interactions between the terrestrial C and N cycles rather than parameterize it in some other way.

Here, we present the implementation of N cycle in the Canadian Land Surface Scheme Including biogeochemical Cycles (CLASSIC) model, which serves as the land component in the family of Canadian Earth System Models (Arora et al., 2009, 2011; Swart et al., 2019). Section 2 briefly describes existing physical and carbon cycle components and processes of the CLASSIC model. The conceptual basis of the new N cycle model and its parameterizations are described

https://doi.org/10.5194/bg-2020-147
Preprint. Discussion started: 14 May 2020

in Section 3 and in the appendix. Section 4 outlines the methodology and data sets that we have used to perform various simulations over the 1850-2017 historical period to assess the realism of the coupled C and N cycles in CLASSIC in response to various forcings. Results from these simulations over the historical period are presented in Section 5 and finally discussion and conclusions are presented in Section 6.

2. The CLASSIC land model

2.1 The physical and carbon biogeochemical processes

The CLASSIC model is the successor to, and based on, the coupled Canadian Land Surface Scheme (CLASS; Verseghy, 1991; Verseghy et al., 1993) and Canadian Terrestrial Ecosystem Model (CTEM; Arora and Boer, 2005; Melton and Arora, 2016). CLASS and CTEM model physical and biogeochemical processes in CLASSIC, respectively. Both CLASS and CTEM have a long history of development as described in Melton et al. (2019) who also provide an overview of the CLASSIC land model and describe its new technical developments that launched CLASSIC as a community model. CLASSIC simulates land-atmosphere fluxes of water, energy, momentum, CO_2, and CH_4. The CLASSIC model can be run at a point scale, e.g. using meteorological and geophysical data from a FluxNet site, or over a spatial domain, that may be global or regional, using gridded data. We briefly summarize the primary physical and carbon biogeochemical processes of CLASSIC here that are relevant in the context of implementation of the N cycle in the model.

2.1.1 Physical processes

The physical processes of CLASSIC that simulate fluxes of water, energy and momentum, based on CLASS, operate at a sub-daily time step. A time step of 30 minutes is typically used to

https://doi.org/10.5194/bg-2020-147
Preprint. Discussion started: 14 May 2020

avoid numerical instabilities. Water, energy, and momentum fluxes are calculated over vegetated, snow, and bare fractions, and the fractional vegetation cover is specified for each grid cell. The vegetation is described in terms of four plant functional types (PFTs) in the operational version of the model: needleleaf trees, broadleaf trees, crops, and grasses. The fractional coverage of these four PFTs are either specified or may be dynamically simulated using competition between PFTs, calculations for which are performed in the biogeochemical module (CTEM). The structural attributes of vegetation are described by leaf area index (LAI), vegetation height, canopy mass, and rooting depth and distribution that determine the fraction of roots in each of the model's soil layers. These structural vegetation attributes may be specified or simulated dynamically by the biogeochemical module of CLASSIC as a function of the driving meteorological data and [CO_2]. The number of permeable soil and non-permeable bedrock layers in CLASSIC can be varied depending on its application. The standard offline model that is driven with reanalysis meteorological data, like in this study, uses 20 ground layers starting with 10 layers of 0.1 m thickness, gradually increasing to a 30 m thick layer for a total ground depth of over 61 m. For application within the Canadian Earth system model currently three ground layers with thicknesses of 0.1, 0.25 and 3.75 m are used. The depth to bedrock varies geographically and is specified based on a soil depth data set. Above this depth, the layers are considered soil and therefore permeable allowing movement of water between the layers for which liquid and frozen soil moisture contents are determined prognostically. Below the permeable soil, the bedrock rock layers are considered impermeable and therefore their soil moisture content is zero. Soil and bedrock temperatures are found for each ground layer. CLASSIC also prognostically models the temperature, mass, albedo, and density of a single layer snow pack (when the climate

https://doi.org/10.5194/bg-2020-147
Preprint. Discussion started: 14 May 2020

permits snow to exist), the temperature and depth of ponded water on the soil, and the temperature of the vegetation canopy. Interception and throughfall of rain and snow by the canopy, and the subsequent unloading of snow, are also modelled. Energy and water balance of each grid cell evolves independently and there is no lateral transfer of heat or moisture between them.

2.1.2 Biogeochemical processes

The biogeochemical processes in CLASSIC are based on CTEM, and described in detail in the appendix of Melton and Arora (2016). The biogeochemical component of CLASSIC simulates the land-atmosphere exchange of CO_2 and while doing so simulates vegetation as a dynamic component. The physics module (CLASS) provides the biogeochemical module (CTEM) with physical land surface information including net radiation, and liquid and frozen soil moisture contents of all the soil layers. The biogeochemical module of CLASSIC uses this information along with air temperature to simulate photosynthesis and prognostically calculates amount of carbon in the model's three live (leaves, stem, and root) and two dead (litter and soil) carbon pools. Photosynthesis in CLASSIC is modelled at the same sub-daily time as the physical processes. The remainder of the biogeochemical processes are modelled at a daily time step. These include: 1) autotrophic and heterotrophic respirations from all the live and dead carbon pools, respectively, 2) allocation of photosynthate from leaves to stem and roots, 3) leaf phenology, 4) turnover of live vegetation components that generates litter, 5) mortality, 6) land use change (LUC), 7) fire (Arora and Melton, 2018), and 8) competition between PFTs for space (not switched on in this study).

https://doi.org/10.5194/bg-2020-147
Preprint. Discussion started: 14 May 2020

172

173 Figure 1 shows the existing structure of CLASSIC's carbon pools along with the addition
174 of non-structural carbohydrate pools for each of the model's live vegetation components. The
175 non-structural pools are not yet represented in the current operational version of CLASSIC
176 (Melton et al., 2019). The addition of non-structural carbohydrate pools is explained in Asaadi et
177 al. (2018) and helps improve leaf phenology for cold deciduous tree PFTs. The N cycle model
178 presented here is built on the research version of CLASSIC that consists of non-structural and
179 structural carbon pools for the leaves (L), stem (S), and root (R) components and the two dead
180 carbon pools in litter or detritus (D) and soil or humus (H) (Figure 1). We briefly describe these
181 carbon pools and fluxes between them, since N cycle pools and fluxes are closely tied to carbon
182 pools and fluxes. The gross primary productivity (GPP) flux enters the leaves from the
183 atmosphere. This non-structural photosynthate is allocated between leaves, stem, and roots. The
184 non-structural carbon then moves into the structural carbohydrates pool. Once this conversion
185 occurs structural carbon cannot be converted back to non-structural labile carbon. The model
186 attempts to maintain a minimum fraction of non-structural to total carbon in each component of
187 about 0.05 (Asaadi et al., 2018). Non-structural carbon is moved from stem and root components
188 to leaves, at the time of leaf onset for deciduous PFTs, and this is termed reallocation. The
189 movement of non-structural carbon is indicated by red arrows. Maintenance and growth
190 respiration (indicated by subscript *m* and *g* in Figure 1), which together constitute autotrophic
191 respiration, occur from the non-structural components of the three live vegetation components.
192 Litterfall from the structural and non-structural components of the vegetation components
193 contributes to the litter pool. Leaf litterfall is generated due to normal turnover of leaves as well

https://doi.org/10.5194/bg-2020-147
Preprint. Discussion started: 14 May 2020

as cold and drought stress, and reduction in day length. Stem and root litter is generated due to their turnover based on their specified life spans. Heterotrophic respiration occurs from the litter and soil carbon pools depending on soil moisture and temperature, and humified litter is moved from litter to the soil carbon pool.

All these terrestrial ecosystem processes and the amount of carbon in the live and dead carbon pools are modelled explicitly for nine PFTs that map directly onto the four base PFTs used in the physics module of CLASSIC. Needleleaf trees are divided into their deciduous and evergreen phenotypes, broadleaf trees are divided into cold deciduous, drought deciduous, and evergreen phenotypes, and crops and grasses are divided based on their photosynthetic pathways into C_3 and C_4 versions. The sub-division of PFTs is required for modelling biogeochemical processes. For instance, simulating leaf phenology requires the distinction between evergreen and deciduous phenotypes of needleleaf and broadleaf trees. However, once LAI is known, a physical process (such as the interception of rain and snow by canopy leaves) does not need to know the underlying evergreen or deciduous nature of leaves.

The prognostically determined biomasses in leaves, stem, and roots are used to calculate structural vegetation attributes that are required by the physics module. Leaf biomass is used to calculate LAI using PFT-dependent specific leaf area. Stem biomass is used to calculate vegetation height for tree and crop PFTs, and LAI is used to calculate vegetation height for grasses. Finally, root biomass is used to calculate rooting depth and distribution which determines the fraction of roots in each soil layer. Other than these structural vegetation attributes the biogeochemical module also calculates canopy resistance (in conjunction with photosynthesis) that is used by the physics module in calculating transpiration.

https://doi.org/10.5194/bg-2020-147
Preprint. Discussion started: 14 May 2020

The approach for calculating photosynthesis in CLASSIC is based on the standard Farquhar et al. (1980) model for C_3 photosynthetic pathway, and Collatz et al. (1992) for the C_4 photosynthetic pathway and presented in detail in Arora (2003). The model calculates gross photosynthesis rate that is co-limited by the photosynthetic enzyme Rubisco, by the amount of available light, and by the capacity to transport photosynthetic products for C_3 plants or the CO_2-limited capacity for C_4 plants. In the real world, the maximum Rubsico limited rate (V_{cmax}) depends on the leaf N content since photosynthetic capacity and leaf N are strongly correlated (Evans, 1989; Field and Mooney, 1986; Garnier et al., 1999). In the current operational version of CLASSIC, the N cycle is not represented and the PFT-dependent values of V_{cmax} are therefore specified based on Kattge et al. (2009) who compile V_{cmax} values using observation-based data from more than 700 measurements. Along with available light, and the capacity to transport photosynthetic products, the GPP in the model is strongly determined by specified PFT-dependent values of $V_{cmax.}$ Also, in the current CLASSIC version a parameterization of photosynthesis downregulation is included which, in the absence of the N cycle, implicitly attempts to simulate the effects of nutrient constraints. This parameterization is explained in detail in Arora et al. (2009) and briefly summarized here.

Following earlier simpler approaches (Cao et al., 2001; Alexandrov and Oikawa, 2002), GPP can be expressed as a logarithmic function of [CO_2]

$$G_p(t) = G_0\left(1 + \gamma_p \ln\frac{c(t)}{c_0}\right) \quad (1)$$

where the unconstrained or potential GPP at any given time, $G_p(t)$, is a function of its initial value G_0, [CO_2] at time t, $c(t)$, and its initial value c_0. The rate of increase of GPP is determined by the

https://doi.org/10.5194/bg-2020-147
Preprint. Discussion started: 14 May 2020

parameter γ_p (where p indicates the "potential" rate of increase of GPP with [CO_2]). The parameter γ_p is calculated by fitting equation (1) to simulated GPP over the historical period. In the absence of any nutrient constraints, the rate of increase of carbon uptake per unit area of leaves is determined by the theoretical framework of Farquhar et al. (1980) and Collatz et al. (1992) for C_3 and C_4 photosynthetic pathways, respectively. The rate of increase of global GPP, however, also depends on how the model simulated LAI increases in response to increasing [CO_2], which in turn depends on how photosynthate is allocated between leaves, stem, and root. Arora et al. (2009) compared the unconstrained simulated rate of increase of GPP per unit increase in [CO_2] (their Figure 3) with that based on the theoretical framework to show that the model's response to increasing [CO_2] over the historical period is consistent with the theoretical framework, given specified time-independent V_{cmax} values for different PFTs. To parameterize downregulation of photosynthesis with increasing [CO_2] for emulating nutrient constraints, the unconstrained or potential GPP (for each time step and each PFT in a grid cell) is multiplied by the global scalar $\xi(c)$

$$G = \xi(c)\, G_p \tag{2}$$

$$\xi(c) = \frac{1+\gamma_d \ln(c/c_0)}{1+\gamma_p \ln(c/c_0)} \tag{3}$$

where t is omitted for clarity and the parameter γ_d represents the downregulated rate of increase of GPP with [CO_2] (indicated by the subscript *d*). When $\gamma_d < \gamma_p$ the modelled gross primary productivity (*G*) increases in response to [CO_2] at a rate determined by the value of γ_d. In the absence of the N cycle, the term $\xi(c)$ thus emulates down-regulation of photosynthesis as CO_2 increases. For example, values of γ_d=0.42 and γ_p=0.90, from Arora et al. (2009), yield a value

https://doi.org/10.5194/bg-2020-147
Preprint. Discussion started: 14 May 2020

of $\xi(c)$ = 0.94 (indicating a 6% downregulation) for c=390 ppm (corresponding to year 2010) and c_0=285 ppm.

Note that while the original model version does not include a N cycle, it is capable of simulating realistic geographical distribution of GPP that partly comes from specification of observation-based V_{cmax} rates (which implicitly take into account C and N interactions in a non-dynamic way) but more so the fact that the geographical distribution of GPP (and therefore net primary productivity, NPP), to the first order, depends on climate. The Miami NPP model, for instance, is able to simulate the geographical distribution of NPP using only mean annual temperature and precipitation (Leith, 1975) since both the C and N cycles are governed primarily by climate. The current version of CLASSIC is also able to reasonably simulate the terrestrial C sink over the second half of the 20th century and early 21st century. CLASSIC (with the CLASS-CTEM name) has regularly contributed to the annual Trends in Net Land–Atmosphere Carbon Exchange (TRENDY) model intercomparison since 2016 which contributes results to the Global Carbon Project's annual assessments – the most recent one being Friedlingstein et al. (2019). What is then the purpose of coupling C and N cycles?

3. Implementation of the N cycle in CLASSIC

The primary objective of implementation of the N cycle is to model V_{cmax} as a function of leaf N content so as to make the use of multiplier $\xi(c)$ obsolete in the model, and allow to project future carbon uptake that is constrained by available N. Modelling of leaf N content as a prognostic variable, however, requires modelling the full N cycle over land. N enters the soil in

https://doi.org/10.5194/bg-2020-147
Preprint. Discussion started: 14 May 2020

the inorganic mineral form through biological fixation of N, fertilizer application, and atmospheric N deposition in the form of ammonium and nitrate. N cycling through plants implies uptake of inorganic mineral N by plants, its return to soil through litter generation in the organic form, and its conversion back to mineral form during decomposition of organic matter in litter and soil. Finally, N leaves the coupled soil-vegetation system through leaching in runoff and through various gaseous forms to the atmosphere. This section describes how these processes are implemented and parameterized in the CLASSIC modelling framework. While the first order interactions between C and N cycles are described well by the current climate, their temporal dynamics over time require to explicitly model these processes.

Globally, terrestrial N cycle processes are even less constrained than the C cycle processes. As a result, the model structure and parameterizations are based on conceptual understanding and mostly empirical observations of N cycle related biological processes. We attempt to achieve balance between a parsimonious and simple model structure and the ability to represent the primary feedbacks and interactions between different model components.

3.1 Model structure, and N pools and fluxes

N is associated with each of the model's five live vegetation components and the two dead carbon pools (shown in Figure 1). In addition, separate mineral pools of ammonium (NH_4^+) and nitrate (NO_3^-) are considered. Figure 2 shows the C and N pools together in one graphic along with the fluxes of N and C between various pools. These fluxes characterize the prognostic nature of the pools as defined by the rate change equations below. The model structure allows the C:N ratio of the live leaves ($C:N_L = C_L/N_L$), stem ($C:N_S = C_S/N_S$), and root ($C:N_R = C_R/N_R$)

https://doi.org/10.5194/bg-2020-147
Preprint. Discussion started: 14 May 2020

components, and the dead litter (or debris) pool ($C{:}N_D = C_D/N_D$) to evolve prognostically. The C:N ratio of soil organic matter ($C{:}N_H = C_H/N_H$), however, is assumed to be constant at 13 following Wania et al. (2012) (see also references therein) . The implications of this assumption are discussed later.

The rates of change of N in the NH_4^+ and NO_3^- pools (in gN m^{-2}), N_{NH4} and N_{NO3}, respectively, are given by

$$\frac{d\,N_{NH4}}{dt} = B_{NH4} + F_{NH4} + P_{NH4} + M_{D,NH4} + M_{H,NH4} - U_{NH4} - (I_{NO3} + I_{N2O} + I_{NO}) - V_{NH3} - O_{NH4} \quad (4)$$

$$\frac{d\,N_{NO3}}{dt} = P_{NO3} + I_{NO3} - L_{NO3} - U_{NO3} - (E_{N2} + E_{N2O} + E_{NO}) - O_{NO3} \quad (5)$$

and all fluxes are represented in units of gN m^{-2} day^{-1}. B_{NH4} is the rate of biological N fixation which solely contributes to the NH_4^+ pool, F_{NH4} is the fertilizer input which is assumed to contribute only to the NH_4^+ pool, and P_{NH4} and P_{NO3} are atmospheric deposition rates that contribute to the NH_4^+ and NO_3^- pools, respectively. Biological N fixation, fertilizer input, and atmospheric deposition are the three routes through which N enters the coupled soil-vegetation system. $M_{D,NH4}$ and $M_{H,NH4}$ are the mineralization flux from the litter and soil organic matter pools, respectively, associated with their decomposition. We assume mineralization of humus and litter pools only contributes to the NH_4^+ pool. O_{NH4} and O_{NO3} indicate immobilization of N from the NH_4^+ and NO_3^- pools, respectively, to the humus N pool which implies microbes (that are not represented explicitly) are part of the humus pool. Combined together the terms ($M_{D,NH4} + M_{H,NH4} - O_{NH4} - O_{NO3}$) yield the net mineralization rate. V_{NH3} is the rate of

https://doi.org/10.5194/bg-2020-147
Preprint. Discussion started: 14 May 2020

ammonia (NH_3) volatilization and L_{NO3} is the leaching of N that occurs only from the NO_3^- pool. The positively charged ammonium ions are attracted to the negatively charged soil particles and as a result it is primarily the negatively charged nitrate ions that leach through the soil (Porporato et al., 2003; Xu-Ri and Prentice, 2008). U_{NH4} and U_{NO3} are uptakes of NH_4^+ and NO_3^- by plants, respectively. The nitrification flux from NH_4 to NO_3 pool is represented by I_{NO3} which also results in the release of the nitrous oxide (N_2O), a greenhouse gas, and nitric oxide (NO) through nitrifier denitrification represented by the terms I_{N2O} and I_{NO}, respectively. Finally, E_{N2}, E_{N2O}, and E_{NO} are the gaseous losses of N_2 (nitrogen gas), N_2O, and NO from the NO_3^- pool associated with denitrification. N is thus lost through the soil-vegetation system via leaching in runoff and through gaseous losses of I_{N2O}, I_{NO}, E_{N2}, E_{N2O}, E_{NO}, and V_{NH3}.

The structural and non-structural N pools in root are written as $N_{R,S}$ and $N_{R,NS}$, respectively, and similarly for stem ($N_{S,S}$ and $N_{S,NS}$) and leaves ($N_{L,S}$ and $N_{L,NS}$), and together the structural and non-structural pools make the total N pool in leaf ($N_L = N_{L,S} + N_{L,NS}$), root ($N_R = N_{R,S} + N_{R,NS}$), and stem ($N_S = N_{S,S} + N_{S,NS}$) components. The rate change equation for structural and non-structural N pools in root are given by

$$\frac{d\,N_{R,NS}}{dt} = U_{NH4} + U_{NO3} + R_{L2R} - R_{R2L} - A_{R2L} - A_{R2S} - LF_{R,NS} - T_{R,NS2S} \quad (6)$$

$$\frac{d\,N_{R,S}}{dt} = T_{R,NS2S} - LF_{R,S} \quad (7)$$

Similar to the uptake of carbon by leaves and its subsequent allocation to root and stem components, N is taken up by roots and then allocated to leaves and stem. A_{R2L} and A_{R2S} represent the allocation of N from roots to leaves and stem, respectively. The terms R_{L2R} and R_{R2L} represent the reallocation of N between the non-structural components of root and leaves.

https://doi.org/10.5194/bg-2020-147
Preprint. Discussion started: 14 May 2020

R_{L2R} is the N reallocated from leaves to root representing resorption of a fraction of leaf N during leaf fall for deciduous tree PFTs. R_{R2L} indicates reallocation of N from roots to leaves (termed reallocation in Figure 2) at the time of leaf-out for deciduous tree PFTs. At times other than leaf-out and leaf-fall and for other PFTs these two terms are zero. $T_{R,NS2S}$ is the one way transfer of N from the non-structural to the structural root pool, and similar to the carbon pools, once N is converted to its structural form it cannot be converted back to its non-structural form. Finally, the litterfall due to turnover of roots occurs from both the structural ($LF_{R,S}$) and non-structural ($LF_{R,NS}$) N pools.

The rate change equations for non-structural and structural components of leaves are written as

$$\frac{d\,N_{L,NS}}{dt} = A_{R2L} - R_{L2R} - R_{L2S} + R_{R2L} + R_{S2L} - LF_{L,NS} - T_{L,NS2S} \quad (8)$$

$$\frac{d\,N_{L,S}}{dt} = T_{L,NS2S} - LF_{L,S} \quad (9)$$

where $T_{L,NS2S}$ is the one way transfer of N from the non-structural leaf component to its structural N pool and R_{S2L} indicates reallocation of N from stem to leaves (similar to R_{R2L}) at the time of leaf out for deciduous tree PFTs. Litterfall occurs from both the structural ($LF_{L,S}$) and non-structural ($LF_{L,NS}$) N pools of leaves, and all other terms have been previously defined.

Finally, the rate change equations for non-structural and structural components of stem are written as

$$\frac{d\,N_{S,NS}}{dt} = A_{R2S} + R_{L2S} - R_{S2L} - LF_{S,NS} - T_{S,NS2S} \quad (10)$$

https://doi.org/10.5194/bg-2020-147
Preprint. Discussion started: 14 May 2020


Biogeosciences Discussions Open Access EGU

$$\frac{d\,N_{S,S}}{dt} = T_{S,NS2S} - LF_{S,S} \tag{11}$$

where $LF_{S,NS}$ and $LF_{S,S}$ represent stem litter from the non-structural and structural components, $T_{S,NS2S}$ is the one way transfer of N from the non-structural stem component to its structural N pool. All other terms have been previously defined.

Adding equations (6) through (11) yields rate of change of N in the entire vegetation pool (N_V) as

$$\begin{aligned} \frac{d\,N_V}{dt} &= \frac{d\,N_{R,NS}}{dt} + \frac{d\,N_{R,S}}{dt} + \frac{d\,N_{L,NS}}{dt} + \frac{d\,N_{L,S}}{dt} + \frac{d\,N_{S,NS}}{dt} + \frac{d\,N_{S,S}}{dt} = \frac{d\,N_R}{dt} + \frac{d\,N_L}{dt} + \frac{d\,N_S}{dt} \\ \frac{d\,N_V}{dt} &= U_{NH4} + U_{NO3} - LF_{R,NS} - LF_{R,S} - LF_{L,NS} - LF_{L,S} - LF_{S,NS} - LF_{S,S} \\ &= U_{NH4} + U_{NO3} - LF_R \qquad\qquad - LF_L \qquad\qquad - LF_S \end{aligned} \tag{12}$$

which indicates how the dynamically varying vegetation N pool is governed by mineral N uptake from the NH_4^+ and NO_3^- pools and litterfall from the structural and non-structural components of the leaves, stem, and root pools. LF_R is the total N litter generation from the root pool and sum of litter generation from its structural and non-structural components ($LF_R = LF_{R,S} + LF_{R,NS}$), and similarly for the leaves (LF_L) and the stem (LF_S) pools.

The rate change equations for the organic N pools in the litter (N_D) and soil (N_H) pools are written as follows.

$$\frac{d\,N_D}{dt} = LF_R + LF_L + LF_S - H_{N,D2H} - M_{D,NH4} \tag{13}$$

$$\frac{d\,N_H}{dt} = H_{N,D2H} + O_{NH4} + O_{NO3} - M_{H,NH4} \tag{14}$$

https://doi.org/10.5194/bg-2020-147
Preprint. Discussion started: 14 May 2020

where $H_{N,D2H}$ is the transfer of humidified organic matter from litter to the soil organic matter pool, and all other terms have been previously defined.

Sections A.1, A.2, and A.3 in the appendix describe how the individual terms of the rate change equations of the 10 prognostic N pools (equations 4 through 11, and equations 13 and 14) are specified or parameterized. The treatment of these terms are briefly described here. Biological N fixation (BNF, B_{NH4}) is parameterized as a function of soil moisture and temperature with higher fixation rate per unit area for agricultural areas than natural vegetation. If externally specified information for ammonium (NH_4^+) and nitrate (NO_3^-) deposition rates is available then it is used otherwise deposition is assumed to be split equally between NH_4^+ and NO_3^-. Externally specified fertilizer application rates are same throughout the year in the tropics (between 30°S and 30°N), given multiple crop rotations in a given year in tropical regions. Between 30° and 90° latitudes in both northern and southern hemispheres, we assume that fertilizer application starts on the spring equinox and ends on the fall equinox. Plant N demand is calculated on the basis of the fraction of NPP allocated to leaves, stem, and root components and their specified minimum PFT-dependent C:N ratios. Both passive and active root uptakes of N are modelled. Passive uptake depends on transpiration and concentration of NH_4^+ and NO_3^- in the root zone water column. When passive N uptake cannot meet the N demand, active uptake compensates for reduced passive uptake though eventually they both depend on the amount of available N in the mineral pools. Plant N uptake by roots is allocated to stem and leaf components, which allows to model leaf N content (N_L) as a prognostic variable. N contributions to litter through litterfall are based on C:N ratios of the vegetation components and the litterfall rates. Resorption of N before litterfall for deciduous tree species is also modelled. Decomposition of litter and soil organic

https://doi.org/10.5194/bg-2020-147
Preprint. Discussion started: 14 May 2020

matter releases C to the atmosphere as CO_2 and the mineralized N is moved to the NH_4^+ pool. Immobilization of mineral N from NH_4^+ and NO_3^- pools into the soil organic matter pool is meant to keep the soil organic matter C:N ratio ($C: N_H$) at its specified constant value of 13 for all PFTs.

Nitrification, the process converting ammonium to nitrate, is driven by microbial activity and depends both on soil temperature and moisture such that it is constrained both at high and low soil moisture contents. Gaseous fluxes of NO (I_{NO}) and N_2O (I_{N2O}) are associated with nitrification and assumed to be directly proportional to the nitrification flux. Denitrification is modelled to reduce NO_3^- to NO, N_2O, and ultimately to N_2. Unlike nitrification, however, denitrification is primarily an anaerobic process and therefore occurs primarily when soil is saturated. Leaching of NO_3^- (L_{NO3}) is parameterized to be directly proportional to baseflow from the bottommost soil layer and the size of the NO_3^- pool. Finally, NH_3 volatilization (V_{NH3}) is parametrized as a function of NH_4^+ pool size, soil temperature, soil pH, and aerodynamic and boundary layer resistances.

3.2 Coupling of C and N cycles

As mentioned earlier in Section 2.1.2, the primary objective of coupling of C and N cycles is to be able to simulate V_{cmax} as a function of leaf N content (N_L) for each PFT. This coupling is represented through the following relationship

$$V_{cmax} = \Gamma_1 N_L + \Gamma_2 \quad (15)$$

where Γ_1 (13 μmol CO_2 gN^{-1} s^{-1}) and Γ_2 (8.5 μmol CO_2 m^{-2} s^{-1}) are global constants, except for the broadleaf evergreen tree PFT for which a lower value of Γ_1 (5.1 μmol CO_2 gN^{-1} s^{-1}) is used as discussed below. A linear relationship between photosynthetic capacity and N_L (Evans, 1989;

https://doi.org/10.5194/bg-2020-147
Preprint. Discussion started: 14 May 2020

Field and Mooney, 1986; Garnier et al., 1999) and between photosynthetic capacity and leaf chlorophyll content (Croft et al., 2017) is empirically observed. The modelled differences in PFT specific values of V_{cmax}, in our framework, come through differences in simulated N_L values that depend on BNF, given that BNF is the primary natural source of N input into the coupled soil-vegetation system. N_L values, however, also depend on leaf phenology, allocation of carbon and nitrogen, turnover rates, transpiration (which brings in N through passive uptake), and almost every aspect of plant biogeochemistry which affects a PFT's net primary productivity and therefore N demand. We have avoided using PFT-dependent values of Γ_1 and Γ_2 for easy optimization of these parameter values but also because such an optimization can potentially hide other model deficiencies. More importantly, using PFT-independent values of Γ_1 and Γ_2 yields a more elegant framework whose successful evaluation will provide confidence in the overall model structure.

As shown later in the results section, using Γ_1 and Γ_2 as global constants yields GPP values that are higher in the tropical region than an observation-based estimate. This is not surprising since tropical regions are well known to be limited by P (Vitousek, 1984; Aragão et al., 2009; Vitousek et al., 2010) and our framework currently doesn't model a P cycle explicitly. An implication of productivity that is limited by P is that changes in N_L are less important. In the absence of explicit treatment of the P cycle, we therefore simply use a lower value of Γ_1 for the broadleaf evergreen tree PFT which, in our modelling framework, exclusively represents a tropical PFT. Although, a simple way to express P limitation, this approach yields the best comparison with observation-based GPP, as shown later.

https://doi.org/10.5194/bg-2020-147
Preprint. Discussion started: 14 May 2020

The second pathway of coupling between the C and N cycles occurs through mineralization of litter and soil organic matter. During periods of higher temperature, heterotrophic C respiration fluxes increase from the litter and soil organic matter pools and this in turn implies an increased mineralization flux (via equation A14 in the appendix) leading to more mineral N available for plants to uptake.

4.0 Methodology

4.1 Model simulations and input data sets

We perform CLASSIC model simulations with the N cycle for the pre-industrial period followed by several simulations for the historical 1851-2017 period to evaluate the model's response to different forcings, as summarized below. The simulation for the pre-industrial period uses forcings that correspond to year 1850 and the model is run for thousands of years until its C and N pools come into equilibrium. The pre-industrial simulation, therefore, yields the initial conditions from which the historical simulations for the period 1851-2017 are launched.

For the historical period, the model is driven with time-varying forcings that include CO_2 concentration, population density (used by the fire module of the model for calculating anthropogenic fire ignition and suppression), land cover, and meteorological data. In addition, for the N cycle module, the model requires time-varying atmospheric N deposition and fertilizer data. The atmospheric CO_2 and meteorological data (CRU-JRA) are same as those used for the TRENDY model intercomparison project for terrestrial ecosystem models for year 2018 (Le Quéré et al., 2018). The CRU-JRA meteorological data is based on 6-hourly Japanese Reanalysis (JRA) adjusted for monthly values based on the Climate Research Unit (CRU) data and available for the

https://doi.org/10.5194/bg-2020-147
Preprint. Discussion started: 14 May 2020

461 period 1901-2017. Since no meteorological data are available for the 1850-1900 period, we use
462 1901-1925 meteorological data repeatedly for this duration and also the pre-industrial spin up.
463 The assumption is that since there is no significant trend in the CRU-JRA data over this period,
464 these data can be reliably used to spin up the model to equilibrium. The land cover data used to
465 force the model are based on a geographical reconstruction of the historical land cover driven by
466 the increase in crop area following Arora and Boer (2010) but using the crop area data prepared
467 for the Global Carbon Project (GCP) 2018 following Hurtt et al. (2006). Since land cover is
468 prescribed, the competition between PFTs for space for the simulations reported here is switched
469 off. The population data for the period 1850-2017 are based on Klein Goldewijk et al. (2017) and
470 obtained from ftp://ftp.pbl.nl/../hyde/hyde3.2/baseline/zip/. The time-independent forcings
471 consist of soil texture and permeable depth data.

472 Time-varying atmospheric N deposition and fertilizer data used over the historical period
473 are also specified as per the TRENDY protocol. The fertilizer data are based on the N_2O model
474 intercomparison project (NMIP) (Tian et al., 2018) and available for the period 1860-2014. For
475 the period before 1860, 1860 fertilizer application rates are used. For the period after 2014,
476 fertilizer application rates for 2014 are used. Atmospheric N deposition data are from input4MIPs
477 (https://esgf-node.llnl.gov/search/input4mips/) and are the same as used by models
478 participating in CMIP6 for the historical period (1850-2014). For years 2015-2017 the N
479 deposition data corresponding to those from representative concentration pathway (RCP) 8.5
480 scenario are used.

481 To evaluate the model's response to various forcings over the historical period we
482 perform several simulations turning on one forcing at a time as summarized in Table 1. The

https://doi.org/10.5194/bg-2020-147
Preprint. Discussion started: 14 May 2020

483 objective of these simulations is to see if the model response to individual forcings is consistent
484 with expectations. For example, in the CO2-only simulation only atmospheric CO_2 concentration
485 increases over the historical period, while all other forcings stay at their 1850 levels. In the N-
486 DEP-only simulation only N deposition increases over the historical period, and similarly for other
487 runs in Table 1. A "FULL" simulations with all forcings turned on is then also performed which we
488 compare to the original model without a N cycle which uses the photosynthesis downregulation
489 parameterization (termed "ORIGINAL" in Table 1).

490 Finally, a separate pre-industrial simulation is also performed that uses the same Γ_1 and
491 Γ_2 globally (FULL-no-implicit-P-limitation). This simulation is used to illustrate the effect of
492 neglecting P limitation for the broadleaf evergreen tree PFT in the tropics.

493 **4.2 Evaluation data sources**

494 We compare globally-summed annual values of N pools and fluxes with observations and
495 other models, and where available their geographical distribution and seasonality. In general,
496 however, much less observation-based data are available to evaluate simulated terrestrial N
497 cycle components than for C cycle components. As a result, N pools and fluxes are primarily
498 compared to results from both observation-based studies and other modelling studies
499 (Bouwman et al., 2013; Fowler et al., 2013; Galloway et al., 2004; Vitousek et al., 2013; Zaehle,
500 2013). Since the primary purpose of the N cycle in our framework is to constrain the C cycle, we
501 also compare globally-summed annual values of GPP and net atmosphere-land CO_2 flux, and their
502 zonal distribution with available observation-based and other estimates. The observation-based
503 estimate of GPP is from Beer et al. (2010), who apply diagnostic models to extrapolate ground-

https://doi.org/10.5194/bg-2020-147
Preprint. Discussion started: 14 May 2020

504 based carbon flux tower observations from about 250 stations to the global scale. Observation-
505 based net atmosphere-land CO_2 flux is from Global Carbon Project's 2019 assessment
506 (Friedlingstein et al., 2019).

507 **5.0 Results**

508 **5.1 N inputs**

509 Figure 3, panel a, shows the global values of simulated BNF from the six primary
510 simulations summarized in Table 1. BNF stays at its pre-industrial value of around 80 Tg N yr^{-1} in
511 the CO2-only, FIRE-only, and N-DEP-only simulations. In the CLIM-only (indicated by magenta
512 coloured line) and the FULL-no-LUC (blue line) simulations the change in climate, associated with
513 increases in temperature and precipitation over the 1901-2017 period (see Figure A1 in the
514 appendix), increases BNF to about 85 Tg N yr^{-1}. In our formulation (equation A1) BNF is positively
515 impacted by increases in temperature and precipitation. The values in parenthesis in Figure 3a
516 legend, and in subsequent panels of this and other figures, show average values over the 1850s,
517 the last 20 years (1998-2017) of the simulations, and the change between these two periods. In
518 the LUC+FERT-only simulation (dark green line) the increase in crop area contributes to an
519 increase in global BNF with a value around 110 Tg N yr^{-1} for the present day, since a higher BNF
520 per unit crop area is assumed than for natural vegetation. Finally, in the FULL simulation (red line)
521 the 1998-2017 average value is around 117 Tg N yr^{-1} due both to changes in climate over the
522 historical period and the increase in crop area. Our present day value of global BNF is broadly
523 consistent with other modelling and data-based studies as summarized is Table 2. Panels c and e
524 in Figure 3 show the decomposition of the total terrestrial BNF into its natural (over non-crop

https://doi.org/10.5194/bg-2020-147
Preprint. Discussion started: 14 May 2020

525 PFTs) and anthropogenic (over C_3 and C_4 crop PFTs) components. The increase in crop area over
526 the historical period decreases natural BNF from its pre-industrial value of 59 to 54 Tg N yr^{-1} for
527 the present day as seen for the LUC+FERT-only simulation (green line) in Figure 3c, while
528 anthropogenic BNF over agricultural area increases from 21 to 56 Tg N yr^{-1} (Figure 3e). Figure 3c
529 and 3e show that the increase in BNF (Figure 3a) in the FULL simulation is caused primarily by an
530 increase in crop area. Our present day values of natural and anthropogenic BNF are also broadly
531 consistent with other modelling and data-based studies as summarized in Table 2.

532 Figure 3, panels b, d, and f, show the global values of externally specified fertilizer input,
533 and deposition of ammonium and nitrate, based on the TRENDY protocol, for the six primary
534 simulations. Ammonium and nitrate deposition, and fertilizer input stay at their pre-industrial
535 level for simulations in which these forcings do not increase over the historical period. As
536 mentioned earlier, N deposition is split evenly into ammonium and nitrate. The present day
537 values of fertilizer input and N deposition are consistent with other estimates available in the
538 literature (Table 2). The fertilizer input rate in the simulation with all forcings except land use
539 change (FULL-no-LUC, blue line), that is with no increase in crop area over its 1850 value, is 50 Tg
540 N yr^{-1} compared to 91 Tg N yr^{-1} in the FULL simulation, averaged over the 1998-2017 period. The
541 additional 41 Tg N yr^{-1} of fertilizer input occurs in the FULL simulation due to the increase in crop
542 area but also due to the increasing fertilizer application rates over the historical period.

543 Figure 4 shows the geographical distribution of simulated BNF, and specified fertilizer
544 application and N deposition rates. The geographical distribution of BNF (Figure 4a) looks very
545 similar to the current distribution of vegetation (not shown) with warm and wet regions showing
546 higher values than cold and dry regions since BNF is parameterized as a function of temperature

https://doi.org/10.5194/bg-2020-147
Preprint. Discussion started: 14 May 2020

547 and soil moisture. Figures 4c and 4e show the split of BNF into its natural and anthropogenic
548 components. Anthropogenic BNF only occurs in regions where crop area exists according to the
549 specified land cover and it exhibits higher values than natural BNF in some regions because of its
550 higher value per unit area (see section A.1.1 in the appendix). In Figure 4b, the fertilizer
551 application rates are concentrated in regions with crop area and with values as high as 16 gN m^{-2}
552 especially in eastern China. The N deposition rates are more evenly distributed than fertilizer
553 applications rates, as would be expected, since emissions are transported downstream from their
554 point sources. Areas with high emissions like the eastern United States, India, eastern China, and
555 Europe, however, still stand out as areas that receive higher N deposition.

556 At the global scale, and for the present day, natural BNF (59 Tg N yr^{-1}) is overwhelmed by
557 anthropogenic sources: anthropogenic BNF (60 Tg N yr^{-1}), fertilizer input (91.7 Tg N yr^{-1}), and
558 atmospheric N deposition increase since the pre-industrial era (~45 Tg N yr^{-1}). Currently humanity
559 fixes more N than the natural processes (Vitousek, 1994).

560 **5.2 C and N pools, fluxes response to historical changes in forcings**

561 To understand the model response to changes in various forcings over the historical
562 period we first look at the evolution of global values of primary C and N pools, and fluxes, shown
563 in Figures 5 through 9. Figure 5a shows the time evolution of global annual GPP values, the
564 primary flux of C into the land surface, for the six primary simulations, the ORIGINAL simulation
565 performed with the model version with no N cycle, and the ORIG-UNCONST simulation with no
566 photosynthesis downregulation (see Table 1). The unconstrained rate of increase in GPP (35.6 Pg
567 C yr^{-1} over the historical period) in the ORIG-UNCONST simulation (dark cyan line) is governed by

https://doi.org/10.5194/bg-2020-147
Preprint. Discussion started: 14 May 2020

568 the standard photosynthesis model equations following Farquhar et al. (1980) and Collatz et al.
569 (1992) for C_3 and C_4 plants, respectively. Downregulation of photosynthesis in the ORIGINAL
570 simulation (purple line) is modelled on the basis of equation (1), while in the FULL simulation (red
571 line) photosynthesis downregulation results from a decrease in V_{cmax} values (Figure 6d) due to a
572 decrease in leaf N content (Figure 6b). We will compare the FULL and ORIGINAL simulations in
573 more detail later. The simulations with individual forcings, discussed below, provide insight into
574 the combined response of GPP to all forcings in the FULL simulation.

575 **5.2.1 Response to increasing CO_2**

576 The response of C and N cycles to increasing CO_2 in the CO2-only simulation (orange line
577 in Figure 5) is the most straightforward to interpret. A CO_2 increase causes GPP to increase by 7.5
578 Pg C yr^{-1} over its pre-industrial value (Figure 5a), which in turn causes vegetation (Figure 5b), leaf
579 (Figure 5c), and soil (Figure 5d) carbon mass to increase as well. The vegetation and leaf N
580 amounts (orange line, Figures 6a and 6b), in contrast, decrease in response to increasing CO_2.
581 This is because N gets locked up in the soil organic matter pool (Figure 6c) in response to an
582 increase in the soil C mass (due to the increasing GPP), litter inputs which are now rich in C (due
583 to CO_2 fertilization) but poor in N (since N inputs are still at their pre-industrial level), and the fact
584 that the C:N ratio of the soil organic matter is fixed at 13. This response to elevated CO_2 which
585 leads to increased C and decreased N in vegetation is consistent with meta-analysis of 75 field
586 experiments of elevated CO_2 (Cotrufo et al., 1998). A decrease in N in leaves (orange line, Figure
587 6b) leads to a concomitant decrease in maximum carboxylation capacity (V_{cmax}) (orange line,
588 Figure 6d) and as a result GPP increases at a much slower rate in the CO2-only simulation than in

https://doi.org/10.5194/bg-2020-147
Preprint. Discussion started: 14 May 2020

589 the ORIG-UNCONST simulation (Figure 5a). Due to the N accumulation in the soil organic matter
590 pool, the NH_4^+ and NO_3^- (Figures 6e and 6f) pools also decrease in size in the CO2-only simulation.

591 Figure 7 shows the time series of N demand, plant N uptake and its split between passive
592 and active N uptakes. The plant N demand in the CO2-only simulation (Figure 7a, orange line)
593 increases from its pre-industrial value of 1512 Tg N/yr to 1639 Tg N/yr for the present day since
594 the increasing C input from increasing GPP requires higher N input to maintain preferred
595 minimum C:N ratio of plant tissues. However, since mineral N pools decrease in size over the
596 historical period (Figures 6e and 6f), the total plant N uptake (Figure 7b) reduces. Passive plant N
597 uptake is directly proportional to pool sizes of NH_4^+ and NO_3^- and therefore it reduces in response
598 to increasing CO_2. Active plant N uptake, which compensates for insufficient passive N uptake
599 compared to the N demand, also eventually starts to decline as it also depends on mineral N pool
600 sizes. The eventual result of increased C supply and reduced N supply is an increase in the C:N
601 ratio of all plant components and litter (Figure 8).

602 Figure 9 shows the net mineralization flux (the net transfer of mineralized N from litter
603 and humus pools to the mineral N pools as a result of the decomposition of organic matter),
604 nitrification (N flux from NH_4^+ to the NO_3^- pool), and the gaseous and leaching losses from the
605 mineral pools. The net mineralization flux reduces in the CO2-only simulation (Figure 9a, orange
606 line) as N gets locked up in the soil organic matter. A reduction in the NH_4^+ pool size implies a
607 reduction in the nitrification flux over the historical period (Figure 9b, orange line). Finally,
608 leaching from the NO_3^- pool (Figure 9c), NH_3 volatilization (Figure 9d), and the gaseous losses
609 associated with nitrification from the NH_4^+ pool (Figure 9e) and denitrification from the NO_3^- pool

https://doi.org/10.5194/bg-2020-147
Preprint. Discussion started: 14 May 2020

610 (Figure 9f) all reduce in response to reduction in pool sizes of NH_4+ and NO_3- in the CO2-only
611 simulation.

612 **5.2.2 Response to changing climate**

613 The perturbation due to climate change alone over the historical period in the CLIM-only
614 (magenta coloured lines in Figures 5-9) simulation is smaller than that due to increasing CO_2. In
615 Figure 5a, changes in climate over the historical period increase GPP slightly by 3.60 Pg C yr^{-1}
616 which in turn slightly increases vegetation (including leaf) C mass (Figure 5b,c). The litter and soil
617 carbon mass (Figure 5d), however, decrease slightly due to increased decomposition rates
618 associated with increasing temperature (see Figure A1). Both the increase in BNF due to
619 increasing temperature (magenta line in Figure 3a), and the reduction in litter and soil N mass
620 (Figure 6c) due to increasing decomposition and higher net N mineralization (Figure 9a, magenta
621 line), make more N available. This results in a slight increase in vegetation and leaf N mass
622 (Figures 6a and 6b) and the NH_4^+ (Figure 6e) pool which is the primary mineral pool in soils under
623 vegetated regions. The global NO_3^- pool, in contrast, decreases in the CLIM-only simulation
624 (Figure 6f) with the reduction primarily occurring in arid regions where the NO_3^- amounts are very
625 large (see Figure 10b that shows the geographical distribution of the primary C and N pools). The
626 geographical distribution of NH_4^+ (Figure 10a) generally follows the geographical distribution of
627 BNF, but with higher values in areas where cropland exists and where N deposition is high. The
628 geographical distribution of NO_3^- (Figure 10b) generally shows lower values than NH_4^+ except in
629 the desert regions where lack of denitrification leads to a large buildup of the NO_3^- pool (see
630 section A3.2 in the appendix). Although Figure 10 shows the geographical distribution of mineral
631 N pools from the FULL simulation, the geographical distribution of pools are broadly similar

https://doi.org/10.5194/bg-2020-147
Preprint. Discussion started: 14 May 2020

between different simulations with obvious differences such as lack of hot spots of N deposition and fertilizer input in simulations in which these forcings stay at their pre-industrial levels. Figure 10 also shows the simulated geographical distribution of C and N pools in the vegetation and soil organic matter. The increase in GPP due to changing climate increases the N demand (Figure 7a, magenta line) but unlike the CO2-only simulation, the plant N uptake increases since the NH_4^+ and NO_3^- pools increase in size over the vegetated area in response to increased BNF (Figure 3a, magenta line). The increase in plant N uptake comes from the increase in passive plant N uptake (Figure 7c) while the active plant N uptake reduces (Figure 7d). Active and passive plant N uptakes are inversely correlated. This is by design since active plant N uptake increases when passive plant N uptake reduces and vice-versa, although eventually both depend on the size of available mineral N pools. Enhancement of plant N uptake due to changes in climate, despite increases in GPP associated with a small increase in V_{cmax} (Figure 6d), leads to a small reduction in the C:N ratio of all plant tissues (Figure 8). The litter C:N, in contrast, shows a small increase since not all N makes its way to the litter as a fraction of leaf N is resorbed from deciduous trees leaves prior to leaf fall (Figure 8e). Finally, the small increase in pool sizes of NH_4^+ and NO_3^- leads to a small increase in leaching, volatilization, and gaseous losses associated with nitrification and denitrification (Figure 9).

5.2.3 Response to N deposition

The simulated response of GPP to changes in N deposition (brown line) over the historical period is smaller than that for CO_2 and climate (Figure 5a). The small increase in GPP of 2.0 Pg C yr^{-1} leads to commensurately small increases in vegetation (Figure 5b) and litter plus soil (Figure 5d) C mass. Vegetation and leaf N mass (Figure 6a,b) also increase in response to N deposition

https://doi.org/10.5194/bg-2020-147
Preprint. Discussion started: 14 May 2020

and so do mineral pools of NH_4^+ and NO_3^- (Figure 6e,f). The increase in GPP in the simulation with N deposition results from an increase in V_{cmax} rates (Figure 6d) associated with an increase in leaf N content (Figure 6b). N demand increases marginally and so does plant N uptake in response to N deposition (Figure 7). As would be intuitively expected, the C:N ratio of the whole plant, its components of leaves, stem, and root, and litter decreases slightly in response to N deposition (Figure 8). Net N mineralization, nitrification, leaching, volatilization, and gaseous losses associated with nitrification and denitrification all increase in response to N deposition (Figure 9).

5.2.4 Response to LUC and fertilizer input

The simulated response to LUC, which reflects an increase in crop area, and increased fertilizer deposition rates over the historical period is shown by dark green lines in Figures 5 through 9. The increase in fertilizer input is a much bigger perturbation to the N cycle system than N deposition. Figure 3 shows that at the global scale the fertilizer inputs increase from 0 to ~92 Tg N/yr over the historical period, while the combined NH_4^+ and NO_3^- N deposition rate increases from around 20 to 65 Tg N/yr. In addition, because of higher per unit area BNF rates over crop area than natural vegetation, the increase in crop area in this simulation leads to an increase in anthropogenic BNF from about 20 to 56 Tg N/yr over the historical period. All together increasing crop area and fertilizer inputs imply an additional ~130 Tg N/yr being input into the terrestrial N cycle at the present day since the pre-industrial period, compared to an increase of only 45 Tg N/yr for the N deposition forcing.

https://doi.org/10.5194/bg-2020-147
Preprint. Discussion started: 14 May 2020

674 The global increase in fertilizer input over the historical period leads to higher NH_4^+ and
675 NO_3^- pools (Figures 6e and 6f). Although both fertilizer and BNF contribute to the NH_4^+ pool, the
676 NO_3^- pool also increases through the nitrification flux (Figure 9b). An increase in crop area over
677 the historical period results in deforestation of natural vegetation that reduces vegetation
678 biomass but also soil carbon mass, since a higher soil decomposition rate is assumed over
679 cropland area (Figures 5b and 5d), consistent with empirical measurements (Wei et al., 2014).
680 Fertilizer application only occurs over crop areas which increases the V_{cmax} rates for crops and, as
681 expected, this yields an increase in globally-averaged V_{cmax} (Figure 6d). A corresponding large
682 increase in leaf N content (Figure 6b) is, however, not seen because vegetation (and therefore
683 leaf) N (Figure 6a,b) is also lost through deforestation. In addition, V_{cmax} is a per unit area rate
684 that is averaged over the whole year while leaf and vegetation N pools are sampled at the end of
685 each year and all crops in the northern hemisphere above 30° N are harvested before the year
686 end. Vegetation N mass, in fact, decreases in conjunction with vegetation C mass (Figure 5b).
687 Plant N demand reduces (Figure 7a) and plant N uptake increases (Figure 7b) driven by crop PFTs
688 in response to fertilizer input, as would be intuitively expected. The increase in plant N uptake
689 comes from the increase in passive N uptake, in response to increases in pool sizes of NH_4^+ and
690 NO_3^- over crop areas, while active plant N uptake decreases since passive uptake can more than
691 keep up with the demand over cropland area. While the C:N ratio of vegetation biomass
692 decreases over cropland area in response to fertilizer input (not shown) this is not seen in the
693 globally-averaged C:N ratio of vegetation (Figure 8a) and its components because C and N are
694 also lost through deforestation and the fact that crop biomass is harvested. The C:N of the global
695 litter pool, however, decreases in response to litter from crops which gets rich in N as fertilizer

https://doi.org/10.5194/bg-2020-147
Preprint. Discussion started: 14 May 2020

696 application rates increase. Finally, in Figure 9, global net N mineralization, nitrification, leaching,
697 volatilization, and gaseous losses associated with nitrification and denitrification all increase by
698 a large amount in response to an increase in fertilizer input.

699 **5.2.5 Response to all forcings**

700 We can now evaluate and understand the simulated response of the FULL simulation to
701 all forcings (red line in Figures 5 through 9). The increase in GPP in the FULL simulation (14.5 Pg
702 C/yr) in Figure 5a over the historical period is driven by GPP increase associated with increase in
703 CO_2 (7.5 Pg C/yr), changing climate (3.6 Pg C/yr), and N deposition (2.0 Pg C/yr). The increases
704 associated with these individual forcings add up to 13.1 Pg C/yr indicating that synergistic effects
705 between forcings contribute to the additional 1.4 Pg C/yr increase in GPP. The changes in
706 vegetation and soil plus litter carbon mass (Figures 5b and 5d) in the FULL simulation are similarly
707 driven by these three factors but, in addition, LUC contributes to decreases in vegetation and soil
708 carbon mass as natural vegetation is deforested to accommodate for increases in crop area.
709 Vegetation and leaf N mass (Figures 6a and 6b) decrease in the FULL simulation driven primarily
710 by the response to increasing CO_2 (orange line compared to the red line) while changes in litter
711 and soil N mass are affected variably by all forcings (Figure 6c). Changes in V_{cmax} (Figure 6d) are
712 similarly affected by all forcings: increasing CO_2 leads to a decrease in globally-averaged V_{cmax}
713 values while changes in climate, N deposition, and fertilizer inputs lead to increases in V_{cmax}
714 values with the net result being a small decrease over the historical period. The increase in global
715 NH_4^+ mass (Figure 6e) in the FULL simulation is driven primarily by the increase in fertilizer input
716 while the changes in NO_3^- mass are the net result of all forcings with no single forcing dominating
717 the response. The increase in N demand (Figure 7a) over the historical period is also driven

https://doi.org/10.5194/bg-2020-147
Preprint. Discussion started: 14 May 2020

718 primarily by the increase in atmospheric CO_2. Plant N uptake (Figure 7b) decreases in response
719 to increasing CO_2 but increases in response to changes in climate, N deposition, and fertilizer
720 inputs such that the net change over the historical is a small decrease. The increase in the C:N
721 ratio of vegetation (Figure 8a) and its components (leaves, stem, and root) is driven primarily by
722 an increase in atmospheric CO_2. Changes in litter C:N in the FULL simulation, in contrast, do not
723 experience dominant influence from any one of the forcings. The simulated change in net N
724 mineralization (Figure 9a) in the FULL simulation, over the historical period, is small since the
725 decrease in net N mineralization due to increasing CO_2 is compensated by the increase caused by
726 changes in climate, N deposition, and fertilizer inputs. The remaining fluxes of nitrification, NO_3^-
727 leaching, NH_3 volatilization, and gaseous losses associated with nitrification and denitrification in
728 the FULL simulation (Figure 9) are all strongly influenced by fertilizer input (green line compared
729 to red line).

730 Table 2 compares simulated values of all primary N pools and fluxes from the FULL
731 simulation with other modelling and quasi observation-based studies. Simulated values are
732 averaged over the 1998-2017 period. Where available, time-periods for other modelling and
733 quasi observation-based studies to which estimates correspond are also noted. For the most part
734 simulated pools and fluxes lie within the range of existing studies with the exception of N_2 and
735 NO emissions that are somewhat higher.

736 **5.2.6 Response to all forcings except LUC**

737 The FULL-no-LUC simulation includes all forcings except LUC (blue line in Figures 5
738 through 9) and corroborates several of the points mentioned above. In this simulation crop area

https://doi.org/10.5194/bg-2020-147
Preprint. Discussion started: 14 May 2020

739 stays at its 1850 value. Figure 3b (blue line) shows increasing global fertilizer input in this
740 simulation despite crop area staying at its 1850 value since fertilizer application rates per unit
741 area increase over the historical period. In the absence of the LUC, vegetation C mass (Figure 5b)
742 and soil plus litter C (Figure 5d) and N (Figure 6c) are higher in the FULL-no-LUC compared to the
743 FULL simulation. N demand (Figure 7a) is slightly higher in FULL-no LUC than in FULL simulation
744 because there is more standing vegetation biomass that is responding to increasing CO_2. The
745 increase in volatilization, leaching, and gaseous losses associated with nitrification and
746 denitrification (Figures 9c-9f) are all primarily caused by increased fertilizer input over the
747 specified 1850 crop area. The increase in N losses associated with these processes, over the
748 historical period, is much lower in the FULL-no-LUC simulation than in the FULL simulation since
749 crop area stays at its 1850 values.

750 **5.3 Comparison of FULL and ORIGINAL simulations**

751 We now compare the results from the FULL simulation that includes the N cycle with that
752 from the ORIGINAL simulation that does not include the N cycle. Both simulations are driven with
753 all forcings over the historical period. Figure 5a shows that the global GPP values in the FULL (red
754 line) and ORIGINAL (purple line) simulations are quite similar although the rate of increase of GPP
755 in the FULL simulation is slightly higher than in the ORIGINAL simulation. As a result, simulated
756 global vegetation biomass is somewhat higher in the FULL simulation (Figure 5b). The simulated
757 global litter and soil carbon mass (Figure 5d) is, however, lower in the FULL simulation (1073 Pg
758 C) compared to the ORIGINAL simulation (1142 Pg C) and this decrease mainly comes from a
759 decrease at higher latitudes (not shown) due to a decrease in GPP (Figure 11a). The lower GPP in
760 the FULL simulation, combined with the slow decomposition at cold high latitudes, results in a

https://doi.org/10.5194/bg-2020-147
Preprint. Discussion started: 14 May 2020

761 lower equilibrium for litter and soil carbon compared with the ORIGINAL simulation. Overall both
762 these estimates are somewhat lower than the bulk density corrected estimate of 1230 Pg C based
763 on the Harmonized World Soil Database (HWSD) v.1.2 (Köchy et al., 2015). Figure 11a shows that
764 the zonal distribution of GPP from the FULL and ORIGINAL simulations, for the 1998-2017 period,
765 compares reasonably well to the observation-based estimate from Beer et al. (2010). The FULL
766 simulation has slightly lower productivity at high-latitudes than the ORIGINAL simulation, as
767 mentioned above. Overall, however, the inclusion of the N cycle does not change the zonal
768 distribution of GPP in the model substantially. Figure 11b compares the zonal distribution of GPP
769 from the pre-industrial simulation (corresponding to 1850s) from the FULL and FULL-with-no-
770 implicit-P-limitation simulations to illustrate the high GPP in the tropics where P and not N
771 limitation affects GPP.

772 Figure 12a compares globally-summed net atmosphere-land CO_2 flux from the FULL,
773 FULL-no-LUC, and ORIGINAL simulations with quasi observation-based estimates from the 2019
774 Global Carbon Project (Friedlingstein et al., 2019). There are two kinds of estimates in Figure 12a
775 from Friedlingstein et al. (2019): the first is the net atmosphere-land CO_2 flux for the decades
776 spanning the 1960s to the 2000s which are shown as rectangular boxes with their corresponding
777 mean values and ranges, and the second is the terrestrial sink from 1959 to 2018 (dark yellow
778 line). Positive values indicate a sink of carbon over land and negative values a source. The
779 difference between the net atmosphere-land CO_2 flux and the terrestrial sink two is that the
780 terrestrial sink minus the LUC emissions yields the net atmosphere-land CO_2 flux. The
781 atmosphere-land CO_2 flux from the FULL-no-LUC simulation (blue line) is directly comparable to
782 the terrestrial sink since 1959, since the FULL-no-LUC simulation includes no LUC, and shows that

https://doi.org/10.5194/bg-2020-147
Preprint. Discussion started: 14 May 2020

783 the simulated terrestrial sink compares fairly well to the estimates from Friedlingstein et al.
784 (2019). Averaged over the period 1959-2017, the modelled and Global Carbon Project values are
785 2.0 and 2.1 Pg C/yr, respectively. The net atmosphere-land CO_2 flux from the FULL simulation
786 mostly lies within the uncertainty range for the five decades considered, although it is on the
787 higher side compared to estimates from Friedlingstein et al. (2019). The reason for this is that
788 LUC emissions in CLASSIC are much lower than observation-based estimates, as discussed below
789 in context of Figure 12c. CLASSIC simulates LUC emissions only in response to changes in crop
790 area whereas changes in pasture area and wood harvesting also contribute to LUC emissions. The
791 net-atmosphere land CO_2 flux from the ORIGINAL simulation compares better with the estimates
792 from Friedlingstein et al. (2019), than the FULL simulation, because the photosynthesis down-
793 regulation parameter in the ORIGINAL simulation has been adjusted despite discrepancies in
794 simulated LUC processes.

795 Figure 12b compares the zonal distribution of simulated net atmosphere-land CO_2 flux
796 from the FULL and ORIGINAL simulations with the model-mean and range from the terrestrial
797 ecosystem models that participated in the 2019 TRENDY model intercomparison and contributed
798 results to 2019 Global Carbon Project (Friedlingstein et al., 2019). The carbon sink simulated by
799 CLASSIC in the northern hemisphere is broadly comparable to the model-mean estimate from
800 the TRENDY models. However, in the tropics CLASSIC simulates a much stronger sink than the
801 model-mean, likely because of its lower LUC emissions.

802 **5.4 Contribution of forcings to land C sink and sources**

https://doi.org/10.5194/bg-2020-147
Preprint. Discussion started: 14 May 2020

803 Figure 12c shows cumulative net atmosphere-land CO_2 flux for the 1850-2017 period from
804 the six primary simulations with N cycle. These simulations facilitate the attribution of carbon
805 uptake and release over the historical period to various forcings. The cumulative terrestrial sink
806 in the FULL-no-LUC simulation for the period 1850-2017 is simulated to be ~153 Pg C and this
807 compares reasonably well with the estimate of 185 ± 50 Pg C for the period 1850-2014 from Le
808 Quéré et al. (2018). Increase in CO_2 (~115 Pg C), change in climate (~3 Pg C), and N deposition
809 (~19 Pg C) all contribute to this terrestrial sink. These three contributions add up to 137 Pg C so
810 the additional 16 Pg C is contributed by the synergistic effects between the three forcings.
811 Quantified in this way, the contribution of increasing CO_2 (15 out of 137 Pg C), climate change (3
812 out of 137 Pg C), and N deposition (19 out of 137 Pg C) to carbon uptake by land over the historical
813 period (1850-2017) is calculated to be 84%, 2%, and 14%., respectively. Cumulative LUC emissions
814 simulated for the period 1850-2017 by CLASSIC can be estimated using a negative cumulative
815 net-atmosphere-land CO_2 flux of ~66 Pg C from the LUC+FERT-only simulation or by the
816 differencing the FULL and FULL-no-LUC simulations (~71 Pg C). While LUC emissions are highly
817 uncertain, both of these estimates are much lower than the 195 ± 75 Pg C estimate from Le Quéré
818 et al. (2018).

819 **6.0 Discussion and conclusions**

820 The interactions between terrestrial C and N cycles are complex and our understanding
821 of these interactions, and their representation in models, is based on empirical observations of
822 various terrestrial ecosystem processes. In this paper, we have evaluated the response of these
823 interactions by perturbing the coupled C and N cycle processes in CLASSIC with one forcing at a
824 time over the historical period: 1) increase in CO_2, 2) change in climate, 3) increase in N

https://doi.org/10.5194/bg-2020-147
Preprint. Discussion started: 14 May 2020

825 deposition, and 4) LUC with increasing fertilizer input. These simulations are easier to interpret
826 and the model response can be evaluated against both our conceptual knowledge as well as
827 empirical observation-based data. Our assumption is that, if the model response to individual
828 forcings is realistic and consistent with expectations based on empirical observations then the
829 response of the model to all forcings combined will also be realistic and easier to interpret,
830 although we do expect and see synergistic effects between forcings.

831 The simulated response of coupled C and N cycles in CLASSIC to increasing atmospheric
832 CO_2 is an increase in the C:N ratio of vegetation components due to an increase in their C content
833 but also a decrease in their N content. This model response is conceptually consistent with a
834 meta-analysis of 75 field experiments of elevated CO_2 as reported in Cotrufo et al. (1998) who
835 find an average reduction in tissue N concentration of 14%. Most studies analyzed in the Cotrufo
836 et al. (1998) meta-analysis used ambient CO_2 of around 350 ppm and elevated CO_2 of around
837 650-700 ppm. In comparison, the vegetation N content in CLASSIC reduces by 18% in response
838 to a gradual increase in atmospheric CO_2 from 285 ppm to 407 ppm (an increase of 122 ppm)
839 over the 1850-2017 period. These two estimates cannot be compared directly - the majority
840 (59%) of Free-Air Carbon dioxide Enrichment (FACE) experiments last less than 3 years (Jones et
841 al., 2014) and the vegetation experiences a large CO_2 change of around 300-350 ppm while the
842 duration of our historical simulation is 167 years and the gradual increase in CO_2 of 122 ppm over
843 the historical period is much smaller.

844 The response of our model to elevated CO_2 is also consistent with the meta-analysis of
845 McGuire et al. (1995) who report an average decrease in leaf N concentration of 21% in response
846 to elevated CO_2 based on 77 studies, which is the primary reason for downregulation of

https://doi.org/10.5194/bg-2020-147
Preprint. Discussion started: 14 May 2020

847 photosynthetic capacity. The simulated decrease in leaf N mass in our study for the CO2-only
848 experiment is also 21% (Figure 6b). Although, the same caveats that apply to the comparison
849 with the Cotrufo et al. (1998) study also apply to this comparison. The decrease in whole plant
850 and leaf N in our results is conceptually consistent with the meta-analyses of McGuire et al.
851 (1995) and Cotrufo et al. (1998). This decrease is, in fact, necessary in our modelling framework
852 to induce the required downregulation of photosynthesis to simulate the land carbon sink
853 realistically over the historical period. However, the decrease in plant N in response to elevated
854 CO_2, found by McGuire et al. (1995) and Cotrufo et al. (1998), is inconsistent with the meta-
855 analysis of Liang et al. (2016) who, in contrast, report an increase in above and belowground
856 plant N pools in response to elevated CO_2 associated with increase in BNF. We are unable to
857 reconcile this difference between the meta-analysis of Liang et al. (2016) and those from McGuire
858 et al. (1995) and Cotrufo et al. (1998). Liang et al. (2016) also report results from short-term (≤ 3
859 years) and long-term (between 3 to 15 years) studies separately (their Figure 3). They show that
860 the increase in total plant and litter N pools become smaller for long-term studies. The difference
861 in time scales of empirical studies and the real world is a caveat that will always make it difficult
862 to evaluate model results over long time scales.

863 The response of C and N cycles to changes in climate in our model is also conceptually
864 realistic. Globally, GPP increases in response to climate that gradually gets warmer and wetter
865 and as a result vegetation biomass increases. Soil carbon mass, however, decreases (despite
866 increase in NPP inputs) since warmer temperatures also increase heterotrophic respiration (not
867 shown). As a result of increased decomposition of soil organic matter, net N mineralization
868 increases and together with increased BNF the overall C:N ratio of vegetation and leaves

https://doi.org/10.5194/bg-2020-147
Preprint. Discussion started: 14 May 2020

869 decreases, which leads to a V_{cmax} increase. The small increase in V_{cmax}, due to the change in
870 climate, thus also contributes to an increase in GPP over and above that due to an increase in
871 temperature solely, and therefore compensates for the amount of carbon lost due to increased
872 soil organic matter decomposition associated with warmer temperatures. This behaviour is
873 consistent with land C cycle models showing a reduction in the absolute value of the strength of
874 the carbon-climate feedback when they include coupling of C and N cycles (Arora et al., 2019).

875 Modelled GPP increases in response to N deposition through an increase in leaf N content
876 and therefore V_{cmax} values. Finally, changes in land use associated with an increase in crop area,
877 and the associated increase in fertilizer application rates lead to the largest increase in NO_3^-
878 leaching, NH_3 volatilization, and gaseous losses associated with nitrification and denitrification
879 among all forcings. Overall, the model response to perturbation by all individual forcings is
880 realistic, conceptually expected, and of the right sign (positive or negative) although it is difficult
881 to evaluate the magnitude of these responses in the absence of directly comparable observation-
882 based estimates.

883 Despite the model responses to individual forcings that appears consistent with our
884 conceptual understanding of coupled C and N cycles, our modelling framework misses an
885 important feedback process that has been observed in the FACE and other experiments related
886 to changes in natural BNF. FACE sites and other empirical studies report an increase in natural
887 BNF rates at elevated CO_2 (McGuire et al., 1995; Liang et al., 2016) and a decrease in natural BNF
888 rates when additional N is applied to soils (Salvagiotti et al., 2008; Ochoa-Hueso et al., 2013). On
889 a broad scale this is intuitively expected but the biological processes behind changes in BNF rates
890 remain largely unclear. A response can still be parameterized even if the underlying physical and

https://doi.org/10.5194/bg-2020-147
Preprint. Discussion started: 14 May 2020

biological processes are not well understood. For instance, Goll et al. (2012) parameterize BNF as an increasing and saturating function of NPP, $BNF = 1.8\left(1.0 - exp(-0.003\,NPP)\right)$. This approach, however, does not account for the driver behind the increase in NPP - increasing atmospheric CO_2, change in environmental conditions (e.g. wetter and warmer conditions), or increased N deposition. Clearly, increasing BNF if the NPP increase is due to N deposition is inconsistent with empirical observations. Over the historical period an increase in atmospheric CO_2 has been associated with an increase in N deposition so to some extent changes in BNF due to both forcings will cancel each other. We realize the importance of changes in BNF, given it is the single largest natural flux of N into the coupled soil-vegetation system, and aim to address this in a future version of the model.

Our framework assumes a constant C:N ratio of 13 for soil organic matter ($C:N_H$), an assumption also made in other models (e.g. (Wania et al., 2012; Zhang et al., 2018). This assumption is also broadly consistent with Zhao et al. (2019) who attempt to model C:N of soil organic matter, among other soil properties, as a function of mean annual temperature and precipitation using machine learning algorithms (their Figure 2h). It is difficult to currently establish if increasing atmospheric CO_2 is changing $C:N_H$ given the large heterogeneity in soil organic C and N densities, and the difficulty in measuring small trends for such large global pools. A choice of a somewhat different value or had we chosen PFT-dependent values of $C:N_H$ is of relatively less importance in this context since the model is spun to equilibrium for 1850 conditions anyway. It is the change in $C:N_H$ over time that is of importance. The assumption of constant $C:N_H$ is key to yielding a decrease in vegetation N mass, and therefore leaf N mass and V_{cmax}, as CO_2 increases in our framework. Without a decrease in V_{cmax} in our modelling

https://doi.org/10.5194/bg-2020-147
Preprint. Discussion started: 14 May 2020

framework, in response to elevated CO_2, we cannot achieve the downregulation noted by McGuire et al. (1995) in their meta-analysis, and the simulated carbon sink over the historical period would be greater than observed as noted above. It is possible that we are simulating the reduction in leaf N mass, in response to elevated CO_2, for a wrong reason in which case our model processes need to be revisited based on additional empirical data. If our assumption of constant or extremely slowly changing $C:N_H$ is indeed severely unrealistic, this necessitates a point of caution that a realistic land carbon sink can be simulated over the historical period with such an assumption.

Related to this assumption is also the fact that we cannot make decomposition rates of soil organic matter a function of its C:N ratio since it is assumed to be a constant. It is well known that after climate, litter and soil organic matter decomposition rates are controlled by their C:N ratio (Manzoni et al., 2008). Litter decomposition rates can still be made a function of its C:N ratio and we aim to do this for a future model version. Since the C:N ratio of litter increases over the historical period, one implication of inclusion of this model feature will be an enhanced land carbon sink over the historical period due to decreasing litter decomposition rates.

The work presented in this study of coupling C and N cycles in CLASSIC yields a framework that we can build upon to make model processes more realistic, test the effect of various model assumptions, parameterize existing processes in other ways, include additional processes, and evaluate model response at FluxNet sites to constrain model parameters.

https://doi.org/10.5194/bg-2020-147
Preprint. Discussion started: 14 May 2020


Biogeosciences Discussions Open Access EGU

Appendix

A1. N inputs

A1.1 Biological N fixation

Biological N fixation (BNF, B_{NH4}) is caused by both free living bacteria in the soil and by bacteria symbiotically living within nodules of host plants' roots. Here, the bacteria convert free nitrogen from the atmosphere to ammonium, which is used by the host plants. Like any other microbial activity, BNF is limited both by drier soil moisture conditions and cold temperatures. Cleveland et al. (1999) attempt to capture this by parameterizing BNF as a function of actual evapotranspiration (AET). AET is a function primarily of soil moisture (through precipitation and soil water balance) and available energy. In places where vegetation exists, AET is also affected by vegetation characteristics including LAI and rooting depth. Here, we parameterize BNF (B_{NH4}, gN m^{-2} day^{-1}) as a function of modelled soil moisture and temperature to depth of 0.5 m following Xu-Ri and Prentice (2008) which yields a very similar geographical distribution of BNF as the Cleveland et al. (1999) approach as seen in Figure 4c.

$$
\begin{aligned}
B_{NH4} &= \left(\sum_c \alpha_c f_c + \sum_n \alpha_n f_n +\right) f(T_{0.5})\, f(\theta_{0.5}) \\
f(T_{0.5}) &= 2^{(T_{0.5}-25)/10} \\
f(\theta_{0.5}) &= \min\left(0, \max\left(1, \frac{\theta_{0.5}-\theta_w}{\theta_{fc}-\theta_w}\right)\right)
\end{aligned}
\tag{A1}
$$

where α_c and α_n (gN m^{-2} day^{-1}) are BNF coefficients for crop (*c*) and non-crop or natural (*n*) PFTs, which are area weighted using the fractional coverages f_c and f_n of crop and non-crop PFTs that are present in a grid cell, $f(T)$ is the dependence on soil temperature based on a Q_{10} formulation and $f(\theta)$ is the dependence on soil moisture which varies between 0 and 1. θ_{fc} and θ_w are the

https://doi.org/10.5194/bg-2020-147
Preprint. Discussion started: 14 May 2020

954 soil moisture at field capacity and wilting points, respectively. $T_{0.5}$ (°C) and $\theta_{0.5}$ (m^3 m^{-3}) in
955 equation (A1) are averaged over the 0.5 m soil depth over which BNF is assumed to occur. We do
956 not make the distinction between symbiotic and non-symbiotic BNF since this requires explicit
957 knowledge of geographical distribution of N fixing PFTs which are not represented separately in
958 our base set of nine PFTs. A higher value of α_c is used compared to α_n to account for the use of
959 N fixing plants over agriculture areas. Biological nitrogen fixation has been an essential
960 component of many farming systems for considerable periods, with evidence for the agricultural
961 use of legumes dating back more than 4,000 years (O'Hara, 1998). A higher α_c than α_n is also
962 consistent with Fowler et al. (2013) who report BNF of 58 and 60 Tg N yr^{-1} for natural and
963 agricultural ecosystems for present day. Since the area of natural ecosystems is about five times
964 the current cropland area it implies BNF rate per unit land area is higher for crop ecosystems than
965 for natural ecosystems. Values of α_c than α_n and other model parameters are summarized in
966 Table A1.

967 Similar to Cleveland et al. (1999), our approach does not lead to a significant change in
968 BNF with increasing atmospheric CO_2, other than through changes in soil moisture and
969 temperature. At least two meta-analyses, however, suggest that an increase in atmospheric CO_2
970 does lead to an increase in BNF through increased symbiotic activity associated with an increase
971 in both nodule mass and number (McGuire et al., 1995; Liang et al., 2016). Models have
972 attempted to capture this by simulating BNF as a function of NPP (Thornton et al., 2007; Wania
973 et al., 2012). The caveat with this approach and the implications of our BNF approach are
974 discussed in Section 6.

975 **A1.2 Atmospheric N deposition**

https://doi.org/10.5194/bg-2020-147
Preprint. Discussion started: 14 May 2020

Atmospheric N deposition is externally specified. The model reads in spatially- and temporally-varying annual deposition rates from a file. Deposition is assumed to occur at the same rate throughout the year so the same daily rate (gN m^{-2} day^{-1}) is used for all days of a given year. If separate information for ammonium (NH_4^+) and nitrate (NO_3^-) deposition rates is available then it is used otherwise deposition is assumed to be split equally between NH_4^+ and NO_3^- (indicated as P_{NH4} and P_{NO3} in equations 4 and 5).

A1.3 Fertilizer application

Geographically and temporally varying annual fertilizer application rates (F_{NH4}) are also specified externally and read in from a file. Fertilizer application occurs over the C_3 and C_4 crop fractions of grid cells. Agricultural management practices are difficult to model since they vary widely between countries and even from farmer to farmer. For simplicity, we assume fertilizer is applied at the same daily fertilizer application rate (gN m^{-2} day^{-1}) throughout the year in the tropics (between 30°S and 30°N), given the possibility of multiple crop rotations in a given year. Between the 30° and 90° latitudes in both northern and southern hemispheres, we assume that fertilizer application starts on the spring equinox and ends on the fall equinox. The annual fertilizer application rate is thus distributed over around 180 days. This provides somewhat more realism, than using the same treatment as in tropical regions, since extra-tropical agricultural areas typically do not experience multiple crop rotations in a given year.

A2. N cycling in plants and soil

Plant roots take up mineral N from soil and then allocate it to leaves and stem to maintain an optimal C:N ratio of each component. Litterfall from vegetation contributes to the litter pool

https://doi.org/10.5194/bg-2020-147
Preprint. Discussion started: 14 May 2020

and decomposition of litter transfers humified litter to the soil organic matter pool. Decomposition of litter and soil organic matter returns mineralized N back to the NH_4^+ pool, closing the soil-vegetation N cycle loop. Both active and passive plant uptakes of N (from both the NH_4^+ and NO_3^- pools) are explicitly modelled. The modelled plant N uptake is a function of its N demand. Higher N demand leads to higher mineral N uptake from soil.

A2.1 Plant N demand

Plant N demand is calculated based on the fraction of NPP allocated to leaves, stem, and root components and their specified minimum PFT-dependent C:N ratios, similar to other models (Xu-Ri and Prentice, 2008; Jiang et al., 2019). The assumption is that plants always want to achieve their desired minimum C:N ratios if enough N is available.

$$\Delta_{WP} = \Delta_L + \Delta_R + \Delta_S$$
$$\Delta_i = \frac{\max\left(0, NPP \,.\, a_{i,C}\right)}{C{:}N_{i,\min}}, \quad i = L, S, R \tag{A2}$$

where the whole plant N demand (Δ_{WP}) is the sum of N demand for the leaves (Δ_L), stem (Δ_S), and root (Δ_R) components, $a_{i,C}$, $i = L, S, R$ is the fraction of NPP (i.e. carbon as indicated by letter C in the subscript) allocated to leaf, stem, and root components, and $C{:}N_{i,\min}, i = L, S, R$ are their specified minimum C:N ratios (see Table A1 for these and all other model parameters). A caveat with this approach when applied at the daily time step, for biogeochemical processes in our model, is that during periods of time when NPP is negative due to adverse climatic conditions (e.g. during winter or drought seasons), the calculated demand is negative. If positive NPP implies there is demand for N, negative NPP cannot be taken to imply that N must be lost from vegetation. As a result, from a plant's perspective, N demand is assumed to be zero during

https://doi.org/10.5194/bg-2020-147
Preprint. Discussion started: 14 May 2020

periods of negative NPP. N demand is also set to zero when all leaves have been shed (i.e., when GPP is zero). At the global scale, this leads to about 15% higher annual N demand than would be the case if negative NPP values were taken into consideration.

A2.2 Passive N uptake

N demand is weighed against passive and active N uptake. Passive N uptake depends on the concentration of mineral N in the soil and the water taken up by the plants through their roots as a result of transpiration. We assume that plants have no control over N that comes into the plant through this passive uptake. This is consistent with existing empirical evidence that too much N in soil will cause N toxicity (Goyal and Huffaker, 1984), although we do not model N toxicity in our framework. If the N demand for the current time step cannot be met by passive N uptake then a plant compensates for the deficit (i.e., the remaining demand) through active N uptake.

The NH_4^+ concentration in the soil moisture within the rooting zone, referred to as [NH_4] (gN gH_2O^{-1}), is calculated as

$$[\mathrm{NH_4}] = \frac{N_{\mathrm{NH4}}}{\sum_{i=1}^{i\leq r_d} 10^6\, \theta_i\, z_i} \quad \text{(A3)}$$

where N_{NH4} is ammonium pool size (gN m^{-2}), θ_i is the volumetric soil moisture content for soil layer *i* (m^3 m^{-3}), z_i is the thickness of soil layer *i* (m), r_d is the soil layer in which the 99% rooting depth lies as dynamically simulated by the biogeochemical module of CLASSIC following Arora and Boer (2003). The 10^6 term converts units of the denominator term to gH_2O m^{-2}. NO_3^- concentration ([NO_3], gN gH_2O^{-1}) in the rooting zone is found in a similar fashion. The

https://doi.org/10.5194/bg-2020-147
Preprint. Discussion started: 14 May 2020

transpiration flux q_t (kgH_2O m^{-2} s^{-1}) (calculated in the physics module of CLASSIC) is multiplied by [NH_4] and [NO_3] (gN gH_2O^{-1}) to obtain passive uptake of NH_4^+ and NO_3^- (gN m^{-2} day^{-1}) as

$$U_{p,NH4} = 86400 \times 10^3 \, \beta \, q_t[\mathrm{NH_4}]$$
$$U_{p,NO3} = 86400 \times 10^3 \, \beta \, q_t[\mathrm{NO_3}] \quad \text{(A4)}$$

where the multiplier 86400× 10^3 converts q_t to units of gH_2O m^{-2} day^{-1}, and β (see Table A1) is the dimensionless mineral N distribution coefficient with value less than 1 that accounts for the fact that NH_4 and NO_3 available in the soil are not well mixed in the soil moisture solution, and not completely accessible to roots, to be taken up by plants.

A2.3 Active N uptake

The active plant N uptake is parameterized as a function of fine root biomass and the size of NH_4^+ and NO_3^- pools in a manner similar to Gerber et al. (2010) and Wania et al (2012). CLASSIC does not explicitly models fine root biomass. We therefore calculate the fraction of fine root biomass using an empirical relationship that is very similar to the relationship developed by Kurz et al. (1996) (their equation 5) but also works below total root biomass of 0.33 Kg C m^{-2} (the Kurz et al. (1996) relationship yields a fraction of fine root more than 1.0 below this threshold). The fraction of fine root biomass (f_r) is given by

$$f_r = 1 - \frac{C_R}{C_R + 0.6} \quad \text{(A5)}$$

where C_R is the root biomass (KgC m^{-2}) simulated by the biogeochemical module of CLASSIC. Equation (A5) yields fine root fraction approaching 1.0 as C_R approaches 0, so at very low root biomass values all roots are considered fine roots. For grasses the fraction of fine root biomass is set to 1. The maximum or potential active N uptake is given by

https://doi.org/10.5194/bg-2020-147
Preprint. Discussion started: 14 May 2020

1058
$$U_{a,pot,\mathrm{NH4}} = \frac{\varepsilon\, f_r\, C_R\, \mathrm{N_{NH4}}}{k_{p,½}\, r_d + \mathrm{N_{NH4}} + \mathrm{N_{NO3}}}$$
$$U_{a,pot,\mathrm{NO3}} = \frac{\varepsilon\, f_r\, C_R\, \mathrm{N_{NO3}}}{k_{p,½}\, r_d + \mathrm{N_{NH4}} + \mathrm{N_{NO3}}} \quad \text{(A6)}$$

1059 where ε is the efficiency of fine roots to take up N per unit fine root mass per day (gN gC^{-1} day^{-1}), $k_{p,½}$ is the half saturation constant (gN m^{-3}), and $\mathrm{N_{NH4}}$ and $\mathrm{N_{NO3}}$ are the ammonium and nitrate pool sizes (gN m^{-2}) as mentioned earlier. Depending on the geographical location and the time of the year, if passive uptake alone can satisfy the plant demand the actual active N uptake of NH_4 ($U_{a,actual,\mathrm{NH4}}$) and NO_3 ($U_{a,actual,\mathrm{NO3}}$) is set to zero. Conversely, during other times both passive and potential active N uptakes may not be able to satisfy the demand and in this case actual active N uptake is equal to its potential rate. At times other than these, the actual active uptake is lower than its potential value. This adjustment of actual active uptake is illustrated in equation (A7).

1068
$$\text{if } \left(\Delta_{WP} \le U_{p,NH4} + U_{p,NO3}\right)$$
$$U_{a,actual,\mathrm{NH4}} = 0$$
$$U_{a,actual,\mathrm{NO3}} = 0$$

$$\text{if } \left(\Delta_{WP} > U_{p,NH4} + U_{p,NO3}\right) \wedge \left(\Delta_{WP} < U_{p,NH4} + U_{p,NO3} + U_{a,pot,\mathrm{NH4}} + U_{a,pot,\mathrm{NH4}}\right)$$
$$U_{a,actual,\mathrm{NH4}} = \left(\Delta_{WP} - U_{p,NH4} - U_{p,NO3}\right) \frac{U_{a,pot,\mathrm{NH4}}}{U_{a,pot,\mathrm{NH4}} + U_{a,pot,\mathrm{NH4}}}$$
$$U_{a,actual,\mathrm{NO3}} = \left(\Delta_{WP} - U_{p,NH4} - U_{p,NO3}\right) \frac{U_{a,pot,\mathrm{NO3}}}{U_{a,pot,\mathrm{NH4}} + U_{a,pot,\mathrm{NH4}}} \quad \text{(A7)}$$

$$\text{if } \left(\Delta_{WP} \ge U_{p,NH4} + U_{p,NO3} + U_{a,pot,\mathrm{NH4}} + U_{a,pot,\mathrm{NO3}}\right)$$
$$U_{a,actual,\mathrm{NH4}} = U_{a,pot,\mathrm{NH4}}$$
$$U_{a,actual,\mathrm{NO3}} = U_{a,pot,\mathrm{NO3}}$$

1069 Finally, the total N uptake (U), uptake of NH_4^+ (U_{NH4}) and NO_3^- (U_{NO3}), are calculated as

https://doi.org/10.5194/bg-2020-147
Preprint. Discussion started: 14 May 2020

$$U = U_{p,NH4} + U_{p,NO3} + U_{a,actual,\mathrm{NH4}} + U_{a,actual,\mathrm{NO3}}$$
$$U_{NH4} = U_{p,NH4} + U_{a,actual,\mathrm{NH4}} \quad \text{(A8)}$$
$$U_{NO3} = U_{p,NO3} + U_{a,actual,\mathrm{NO3}}$$

A2.4 Litterfall

Nitrogen litterfall from the vegetation components is directly tied to the carbon litterfall calculated by the phenology module of CLASSIC through their current C:N ratios.

$$LF_i = \frac{(1-r_L)LF_{i,C}}{C{:}N_i}, i = L, S, R \quad \text{(A9)}$$

where $LF_{i,C}$ is the carbon litterfall rate (gC day^{-1}) for component *i*, calculated by the phenology module of CLASSIC, and division by its current C:N ratio yields the nitrogen litterfall rate, r_L is the leaf resorption coefficient that simulates the resorption of N from leaves of deciduous tree PFTs before they are shed and $r_i = 0, i = R, S$. Litter from each vegetation component is proportioned between structural and non-structural components according to their pool sizes.

A2.5 Allocation and reallocation

Plant N uptake by roots is allocated to leaves and stem to satisfy their N demand. When plant N demand is greater than zero, total N uptake (U) is divided between leaves, stem, and root components in proportion to their demands such that the allocation fractions for N ($a_i, i = L, S, R$) are calculated as

$$a_i = \frac{\Delta_i}{\Delta_{WP}}, i = L, S, R$$
$$A_{R2L} = a_L\,(U_{NH4} + U_{NO3}) \quad \text{(A10)}$$
$$A_{R2S} = a_S\,(U_{NH4} + U_{NO3})$$

https://doi.org/10.5194/bg-2020-147
Preprint. Discussion started: 14 May 2020

where A_{R2L} and A_{R2S} are the amounts of N allocated from root to leaves and stem components, respectively, as mentioned in the main text for equation (8). During periods of negative NPP due to adverse climatic conditions (e.g. during winter or drought seasons) the plant N demand is set to zero but passive N uptake, associated with transpiration, may still be occurring if the leaves are still on. Even though there is no N demand, passive N uptake still needs to be partitioned among the vegetation components. During periods of negative NPP allocation fractions for N are, therefore, calculated in proportion to the minimum PFT-dependent C:N ratios of the leaves, stem, and root components as follows.

$$a_i = \frac{1/C{:}N_{i,\min}}{1/C{:}N_{L,\min}+1/C{:}N_{S,\min}+1/C{:}N_{R,\min}}, i = L,S,R \quad \text{(A11)}$$

For grasses, which do not have a stem component, equations (A10) and (A11) are modified accordingly by removing the terms associated with the stem component.

Three additional rules override these general allocation rule specifically for deciduous tree PFTs (or deciduous PFTs in general). First, no N allocation is made to leaves once leaf fall is initiated for deciduous tree PFTs and plant N uptake is proportioned between stem and root components based on their demands in a manner similar to equation (A10). Second, for deciduous tree PFTs, a fraction of leaf N is resorbed from leaves back into stem and root as follows

$$R_{L2R} = r_L\, LF_L \frac{N_{R,NS}}{N_{R,NS}+N_{S,NS}}$$
$$R_{L2S} = r_L\, LF_L \frac{N_{S,NS}}{N_{R,NS}+N_{S,NS}} \quad \text{(A12)}$$

https://doi.org/10.5194/bg-2020-147
Preprint. Discussion started: 14 May 2020

where r_L is the leaf resorption coefficient, as mentioned earlier, and LF_L is the leaf litter fall rate. Third, and similar to resorption, at the time of leaf onset for deciduous tree PFTs, N is reallocated to leaves (in conjunction with reallocated carbon as explained in Asaadi et al. (2018)) from stem and root components.

$$R_{R2L} = \frac{R_{R2L,C}}{C{:}N_L} \frac{N_{R,NS}}{N_{R,NS}+N_{S,NS}}$$
$$R_{S2L} = \frac{R_{S2L,C}}{C{:}N_L} \frac{N_{S,NS}}{N_{R,NS}+N_{S,NS}} \quad \text{(A13)}$$

where $R_{R2L,C}$ and $R_{S2L,C}$ represent reallocation of carbon from non-structural stem and root components to leaves and division by $C{:}N_L$ converts the flux into N units. The reallocation demand for N, at the time of leaf onset, is proportioned between non-structural pools of stem and root according to their sizes.

A2.6 N mineralization, immobilization, and humification

Decomposition of litter ($R_{h,D}$) and soil organic matter ($R_{h,H}$) releases C to the atmosphere and this flux is calculated by the heterotrophic respiration module of CLASSIC. The amount of N mineralized is calculated straightforwardly by division with the current C:N ratios of the respective pools and contributes to the NH_4^+ pool.

$$M_{D,NH4} = \frac{R_{h,D}}{C{:}N_D}$$
$$M_{H,NH4} = \frac{R_{h,H}}{C{:}N_H} \quad \text{(A14)}$$

An implication of mineralization contributing to the NH_4^+ pool, in addition to BNF and fertilizer inputs that also contribute solely to the NH_4^+ pool, is that the simulated NH_4^+ pool is typically

https://doi.org/10.5194/bg-2020-147
Preprint. Discussion started: 14 May 2020

larger than the NO_3^- pool. The exception is the dry and arid regions where the lack of denitrification, as discussed below in Section A.3.2., leads to a build up of the NO_3^- pool.

Immobilization of mineral N from the NH_4^+ and NO_3^- pools into the soil organic matter pool is meant to keep the soil organic matter C:N ratio ($C:N_H$) at its specified value of 13 for all PFTs in a manner similar to Wania et al. (2012) and Zhang et al. (2018). A value of 13 is within the range of observation-based estimates which vary from about 8 to 25 (Zinke et al., 1998; Tipping et al., 2016). Although $C:N_H$ varies geographically, the driving factors behind this variability remain unclear. It is even more difficult to establish if increasing atmospheric CO_2 is changing $C:N_H$ given the large heterogeneity in soil organic C and N densities, and the difficulty in measuring small trends for such large global pools. We therefore make the assumption that the $C:N_H$ does not change with time. An implication of this assumption is that as GPP increases with increasing atmospheric CO_2 rises, and plant litter becomes enriched in C with increasing C:N ratio of litter, more and more N is locked up in the soil organic matter pool because its C:N ratio is fixed. As a result, mineral N pools of NH_4^+ and NO_3^- decrease in size and plant N content subsequently follows. This is consistent with studies of plants grown in elevated CO_2 environment. For example, Cotrufo et al. (1998) summarize results from 75 studies and find an average 14% reduction in N concentration for above-ground tissues. Wang et al. (2019) find increased C concentration by 0.8–1.2% and a reduction in N concentration by 7.4–10.7% for rice and winter wheat crop rotation system under elevated CO_2.

Immobilization from both the NH_4^+ and NO_3^- pools is calculated in proportion to their pool sizes, employing the fixed $C:N_H$ ratio as

https://doi.org/10.5194/bg-2020-147
Preprint. Discussion started: 14 May 2020

$$O_{NH4} = \max\left(0, \left(\frac{C_H}{C{:}N_H} - N_H\right)\frac{N_{NH4}}{N_{NH4}+N_{NO3}}\right)$$
$$O_{NO3} = \max\left(0, \left(\frac{C_H}{C{:}N_H} - N_H\right)\frac{N_{NO3}}{N_{NH4}+N_{NO3}}\right) \quad \text{(A15)}$$

Finally, the carbon flux of humified litter from the litter to the soil organic matter pool ($H_{C,D2H}$) is also associated with a corresponding N flux that depends on the C:N ratio of the litter pool.

$$H_{N,D2H} = \frac{H_{C,D2H}}{C{:}N_D} \quad \text{(A16)}$$

A3. N cycling in mineral pools and N outputs

This section presents the parameterizations of nitrification (which results in transfer of N from the NH_4^+ to the NO_3^- pool) and the associated gaseous fluxes of N_2O and NO (referred to as nitrifier denitrification), gaseous fluxes of N_2O, NO, and N_2 associated with denitrification, volatilization of NH_4 into NH_3, and leaching of NO_3^- in runoff.

A3.1 Nitrification

Nitrification, the oxidative process converting ammonium to nitrate, is driven by microbial activity and as such constrained both by high and low soil moisture (Porporato et al., 2003). At high soil moisture content there is little aeration of soil and this constrains aerobic microbial activity, while at low soil moisture content microbial activity is constrained by moisture limitation. In CLASSIC, the heterotrophic respiration from soil carbon is constrained similarly but rather than using soil moisture the parameterization is based on soil matric potential (Arora, 2003; Melton et al., 2015). Here, we use the exact same parameterization. In addition to soil moisture, nitrification (gN m^{-2} day^{-1}) is modelled as a function of soil temperature and the size of the NH_4^+ pool as follows

https://doi.org/10.5194/bg-2020-147
Preprint. Discussion started: 14 May 2020


Biogeosciences Discussions Open Access EGU

$$I_{NO3} = \eta\, f_I(T_{0.5}) f_I(\psi)\, N_{NH4} \quad \text{(A17)}$$

where η is the nitrification coefficient (day^{-1}), $f_I(\psi)$ is the dimensionless soil moisture scalar that varies between 0 and 1 and depends on soil matric potential (ψ), $f_I(T_{0.5})$ is the dimensionless soil temperature scalar that depends on average soil temperature ($T_{0.5}$) over the top 0.5 m soil depth over which nitrification is assumed to occur (following Xu-Ri and Prentice, 2008), and N_{NH4} is the ammonium pool size (gN m^{-2}), as mentioned earlier. Both $f_I(T_{0.5})$ and $f_I(\psi)$ are parameterized following Arora (2003) and Melton et al. (2015). $f_I(T_{0.5})$ is a Q_{10} type function with a temperature dependent Q_{10}

$$f_I(T_{0.5}) = Q_{10,I}^{(T_{0.5}-20)/10},\ Q_{10,I} = 1.44 + 0.56\left(\tanh\left(0.075(46 - T_{0.5})\right)\right) \quad \text{(A18)}$$

The reference temperature for nitrification is set to 20 °C following Lin et al. (2000). $f_I(\psi)$ is parameterized as a step function of soil matric potential (ψ) as

$$f_I(\psi) = \begin{cases} 0.5 & \text{if } \psi \le \psi_{sat} \\ 1 - 0.5\frac{\log(0.4)-\log(\psi)}{\log(0.4)-\log(\psi_{sat})} & \text{if } 0.4 > \psi \ge \psi_{sat} \\ 1 & \text{if } 0.6 \ge \psi \ge 0.4 \\ 1 - 0.8\frac{\log(\psi)-\log(0.6)}{\log(100)-\log(0.6)} & \text{if } 100 > \psi > 0.6 \\ 0.2 & \text{if } \psi > 100 \end{cases} \quad \text{(A19)}$$

where the soil matric potential (ψ) is found, following Clapp and Hornberger (1978), as a function of soil moisture (θ)

$$\psi(\theta) = \psi_{sat}\left(\frac{\theta}{\theta_{sat}}\right)^{-B}. \quad \text{(A20)}$$

Saturated matric potential (ψ_{sat}), soil moisture at saturation (i.e. porosity) (θ_{sat}), and the parameter B are calculated as functions of percent sand and clay in soil following Clapp and

https://doi.org/10.5194/bg-2020-147
Preprint. Discussion started: 14 May 2020

Hornberger (1978) as shown in Melton et al. (2015). The soil moisture scalar $f_I(\psi)$ is calculated individually for each soil layer and then averaged over the soil depth of 0.5 m over which nitrification is assumed to occur.

Gaseous fluxes of NO (I_{NO}) and N_2O (I_{N2O}) associated with nitrification, and generated through nitrifier denitrification, are assumed to be directly proportional to the nitrification flux (I_{NO3}) as

$$\begin{aligned} I_{NO} &= \eta_{NO}\ I_{NO3} \\ I_{N2O} &= \eta_{N2O}\ I_{NO3} \end{aligned}. \quad \text{(A21)}$$

where η_{NO} and η_{N2O} are dimensionless fractions which determine what fractions of nitrification flux are emitted as NO and N_2O.

A3.2 Denitrification

Denitrification is the stepwise microbiological reduction of nitrate to NO, N_2O, and ultimately to N_2 in complete denitrification. Unlike nitrification, however, denitrification is primarily an anaerobic process (Tomasek et al., 2017) and therefore occurs when soil is saturated. As a result, we use a different soil moisture scalar than for nitrification. Similar to nitrification, denitrification is modelled as a function of soil moisture, soil temperature and the size of the NO_3^- pool as follows to calculate the gaseous fluxes of NO, N_2O, and N_2.

$$\begin{aligned} E_{NO} &= \mu_{NO}\ f_E(T_{0.5})\ f_E(\theta)\ N_{NO3} \\ E_{N2O} &= \mu_{N2O}\ f_E(T_{0.5})\ f_E(\theta)\ N_{NO3} \\ E_{N2} &= \mu_{N2}\ f_E(T_{0.5})\ f_E(\theta)\ N_{NO3} \end{aligned} \quad \text{(A22)}$$

where μ_{NO}, μ_{N2O}, and μ_{N2} are coefficients (day^{-1}) that determine daily rates of emissions of NO, N_2O, and N_2. The temperature scalar $f_E(T_{0.5})$ is exactly the same as the one for nitrification

https://doi.org/10.5194/bg-2020-147
Preprint. Discussion started: 14 May 2020


Biogeosciences Discussions Open Access EGU

1199 $(f_l(T_{0.5}))$ since denitrification is also assumed to occur over the same 0.5 soil depth. The soil
1200 moisture scalar $f_E(\theta)$ is given by

1201
$$f_E(\theta) = 1 - \tanh\left(2.5\left(\frac{1-w(\theta)}{1-w_d}\right)^2\right)$$
$$w(\theta) = \max\left(0, \min\left(1, \frac{\theta-\theta_w}{\theta_f-\theta_w}\right)\right) \quad \text{(A23)}$$

1202 where w is the soil wetness that varies between 0 and 1 as soil moisture varies between wilting
1203 point (θ_w) and field capacity (θ_f), and w_d is the threshold soil wetness for denitrification below
1204 which very little denitrification occurs. Since very little denitrification occurs when soil wetness
1205 is below w_d this leads to build up of the NO_3^- pool in arid regions.

1206 **A3.3 NO_3^- leaching**

1207 Leaching is the loss of water-soluble ions through runoff. In contrast to positively charged
1208 NH_4^+ ions (i.e. cations), the NO_3^- ions do not bond to soil particles because of the limited exchange
1209 capacity of soil for negatively charged ions (i.e. anions). As a result, leaching of N in the form of
1210 NO_3^- ions is a common water quality problem, particularly over cropland regions. The leaching
1211 flux (L_{NO3}, gN m^{-2} day^{-1}) is parameterized to be directly proportional to baseflow (b_t, Kg m^{-2} s^{-1}) calculated by the physics module of CLASSIC and the size of the NO_3 pool (N_{NO3}, gN m^{-2}).
1213 Baseflow is the runoff rate from the bottommost soil layer.

1214
$$L_{NO3} = 86400\ \varphi\ b_t\ N_{NO3} \quad \text{(A24)}$$

1215 where the multiplier 86400 converts units to per day, and φ is the leaching coefficient (m^2 Kg^{-1})
1216 that can be thought of as the soil particle surface area (m^2) that 1 Kg of water (or about 0.001
1217 m^3) can effectively wash to leach the nutrients.

https://doi.org/10.5194/bg-2020-147
Preprint. Discussion started: 14 May 2020

A3.4 NH_3 volatilization

NH_3 volatilization (V_{NH3}, gN m^{-2} day^{-1}) is parametrized as a function of pool size of NH_4^+, soil temperature, soil pH, aerodynamic and boundary layer resistances, and atmospheric NH_3 concentration in a manner similar to Riddick et al. (2016) as

$$V_{NH4} = \vartheta \ 86400 \ \frac{1}{r_a + r_b}\left(\chi - [\mathrm{NH_{3,a}}]\right) \quad \text{(A25)}$$

where ϑ is the dimensionless NH_3 volatilization coefficient which is set to less than 1 to account for the fact that a fraction of ammonia released from the soil is captured by vegetation, r_a (s m^{-1}) is the aerodynamic resistance calculated by the physics module of CLASSIC, χ is the ammonia (NH_3) concentration at the interface of the top soil layer and the atmosphere (g m^{-3}), $[\mathrm{NH_{3,a}}]$ is the atmospheric NH_3 concentration specified at 0.3×10^{-6} g m^{-3} following Riddick et al. (2016), 86400 converts flux units from gN m^{-2} s^{-1} to gN m^{-2} day^{-1}, and r_b (s m^{-1}) is the boundary layer resistance calculated following Thom (1975) as

$$r_b = 6.2 \ u_*^{-0.67} \quad \text{(A26)}$$

where u_* (m/s) is the friction velocity provided by the physics module of CLASSIC. The ammonia (NH_3) concentration at surface (χ), in a manner similar to Riddick et al. (2016), is calculated as

$$\chi = 0.26 \frac{N_{NH4}}{1 + K_H + K_H[H^+]/K_{NH4}} \quad \text{(A27)}$$

where the coefficient 0.26 is the fraction of ammonium in the top 10 cm soil layer assuming exponential distribution of ammonium along the soil depth (given by $3e^{-3z}$, where z is the soil depth), K_H (dimensionless) is the Henry's law constant for NH_3, K_{NH4} (mol L^{-1}) is the dissociation equilibrium constant for aqueous NH_3, and H^+ (mol L^{-1}) is the concentration of hydrogen ion

https://doi.org/10.5194/bg-2020-147
Preprint. Discussion started: 14 May 2020

that depends on the soil pH ($H^+ = 10^{-pH}$). K_H and K_{NH4} are modelled as functions of soil temperature of the top 10 cm soil layer ($T_{0.1}$) following Riddick et al. (2016) as

$$K_H = 4.59\, T_{0.1} \exp\left(4092\, \left(\frac{1}{T_{0.1}} - \frac{1}{T_{ref,v}}\right)\right)$$

$$K_{NH4} = 5.67\, \times 10^{-10} \exp\left(-6286\, \left(\frac{1}{T_{0.1}} - \frac{1}{T_{ref,v}}\right)\right) \quad \text{(A28)}$$

where $T_{ref,v}$ is the reference temperature of 298.15 K.

Acknowledgments

We are grateful and thank Joe Melton and Paul Bartlett for their comments on an earlier version of this manuscript.

Code/Data availability

Model code for the operational CLASSIC model can be obtained from https://gitlab.com/cccma/classic. Changes made to the operational version to include N cycle and the results shown here can be obtained from the second author.

Author contributions

A.A. implemented the N cycle in the CLASSIC code, put together all the N cycle related input data, and performed all the simulations. V.A. and A.A. wrote the manuscript.

Competing interests

There are no competing interests.

https://doi.org/10.5194/bg-2020-147
Preprint. Discussion started: 14 May 2020

Biogeosciences
Discussions
Open Access
EGU

1260

1261

1262

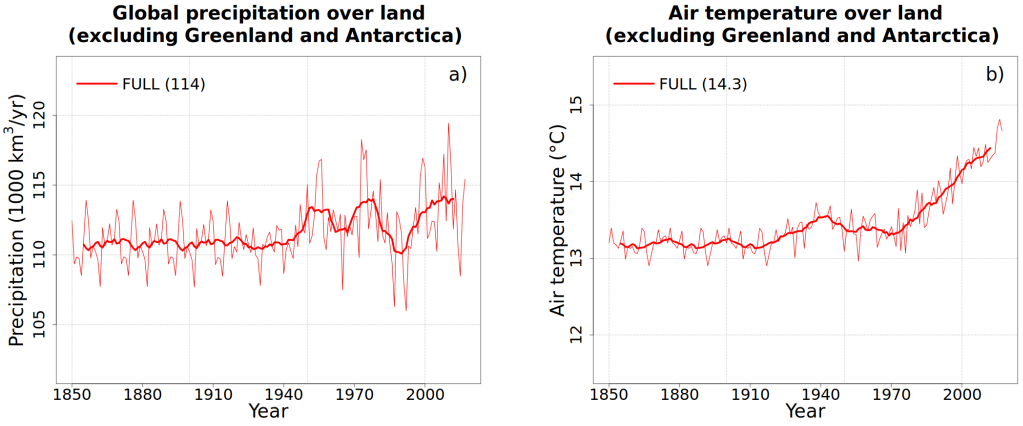

1263

1264

1265 Figure A1: Annual values of global precipitation (a) and air temperature (b) over land in the
1266 CRU-JRA reanalysis data that are used to drive the model. The data are available for the period
1267 1901-2017. In the absence of meterological data, the period 1851-1900 uses the data from the
1268 period 1901-1925 twice.

1269

https://doi.org/10.5194/bg-2020-147
Preprint. Discussion started: 14 May 2020

Table A1: Model parameters for various model parameterizations. Model parameters may be scalar or an array (if they are PFT dependent) in which they are follow the following structure.

Needleleaf evergreen	Needleleaf deciduous	
Broadleaf evergreen	Broadleaf deciduous cold	Broadleaf deciduous drought
C_3 crop	C_4 crop	
C_3 grass	C_4 grass	

Corresponding equation in which the parameter appears in the main text is also noted.

Model parameter	Eqn	Description	Units	Value(s)
Biological N fixation				
α_c	A1	BNF rate for crop PFTs	gN m^{-2} day^{-1}	0.00217
α_n	A1	BNF rate for natural PFTs	gN m^{-2} day^{-1}	0.00037
Plant N demand				
$C:N_{L,min}$	A2	Minimum C:N ratio for leaves	dimensionless	25 22 20 18 18 16 20 13 18
$C:N_{S,min}$	A2	Minimum C:N ratio for stem	dimensionless	450 450 430 430 430 285 285 – –
$C:N_{R,min}$	A2	Minimum C:N ratio for root	dimensionless	45 45 35 35 35 30 35 30 35
Plant uptake				
β	A4	Mineral N distribution coefficient	dimensionless	0.5
ε	A6	Fine root efficiency	gN gC^{-1} day^{-1}	4.92E-5
$k_{p,½}$	A6	Half saturation constant	gN m^{-3}	3
Litterfall				
r_L	A9	Leaf resorption coefficient	dimensionless	0.54
Nitrification				
η	A17	Nitrification coefficient	day^{-1}	7.33E-4

https://doi.org/10.5194/bg-2020-147
Preprint. Discussion started: 14 May 2020

η_{NO}	A21	Fraction of nitrification flux emitted as NO	dimensionless	7.03E-5
η_{N2O}	A21	Fraction of nitrification flux emitted as N_2O	dimensionless	2.57E-5
Denitrification				
μ_{NO}	A22	Fraction of denitrification flux emitted as NO	day^{-1}	3.872E-4
μ_{N2O}	A22	Fraction of denitrification flux emitted as N_2O	day^{-1}	1.408E-4
μ_{N2}	A22	Fraction of denitrification flux emitted as N_2	day^{-1}	3.872E-3
w_d	A23	Soil wetness threshold below which very little denitrification occurs	dimensionless	0.3
Leaching				
φ	A24	Leaching coefficient	$m^2\ Kg^{-1}$	1.15E-3
NH_3 volatilization				
ϑ	A25	NH_3 volatilization coefficient	dimensionless	1.8
Coupling of C and N cycles				
Γ_1	15	Parameter for calculating V_{cmax} from leaf N content	$\mu mol\ CO_2\ gN^{-1}\ s^{-1}$	13 (all PFTs except broadleaf evergreen tree) 5.1 (for broadleaf evergreen tree)
Γ_2	15	Parameter for calculating V_{cmax} from leaf N content	$\mu mol\ CO_2\ m^{-2}\ s^{-1}$	8.5

1275

1276

https://doi.org/10.5194/bg-2020-147
Preprint. Discussion started: 14 May 2020


Biogeosciences Discussions Open Access EGU

1277

1278 **Table 1**: Historical simulations performed over the period 1851-2017 to evaluate the model's
1279 response to various forcings. All forcings are time varying. All forcings are also spatially explicit
1280 except atmospheric CO_2 for which a globally constant value is specified.

1281

Simulation name	Forcing that varies over the historical period	N cycle
Primary simulations performed to evaluate N cycle response to various forcings		
1. CO2-only	Atmospheric CO_2 concentration	Runs with N cycle
2. CLIM-only	1901-1925 meteorological data are used twice over the 1850-1900 period. For the 1901-2017 period, meteorological data for the correct year is used.	
3. LUC+FERT-only	Land cover with increasing crop area, and fertilizer application rates over the crop area	
4. N-DEP-only	N deposition of ammonia and nitrate	
5. FULL	All forcings	
6. FULL-no-LUC	All forcings except increasing crop area	
Other simulations		
7. ORIGINAL	All forcings	Runs without N cycle using the original model configuration.
8. ORIG-UNCONST	All forcings but with downregulation turned off	
9. FULL-no-implicit-P-limitation	All forcings but using same Γ_1 and Γ_2 globally	Run with N cycle

1282

1283

1284

https://doi.org/10.5194/bg-2020-147
Preprint. Discussion started: 14 May 2020

1285 **Table 2**: Comparison of simulated global N pools and fluxes, from the FULL simulation, with other
1286 modelling and quasi observation-based studies (references for which are noted as superscripts
1287 and listed below the table). The time-periods to which the other modelling and quasi
1288 observation-based estimates correspond are also noted, where available. The estimates are for
1289 land. Simulated fluxes and pool corresponds to the period 1997-2018.

1290

N pool and fluxes	This study (1998-2017)	Other model and quasi observation-based estimates
N inputs (Tg N yr^{-1})		
BNF	119	118[a] 99[b] (2001-2010) 138.5[c] (early 1990s) 128.9[d] (2000-2009) 104-118[e] 92[f] (year 2000)
Natural BNF	59	58[a] 107[c] (early 1990s) 30-130[e] 39[f] (year 2000)
Anthropogenic BNF	60	60[a] 31.5[c] (early 1990s) 14-89[e] 53[f] (year 2000)
Fertilizer input	91 (based on TRENDY protocol)	100[a] 100[b] (2001-2010) 100[c] (early 1990s) 83[f] (year 2000)
N deposition	66 (based on TRENDY protocol)	70[a] 56-62[b] 63.5[c] (early 1990s) 69[f] (year 2000)
N pools (Tg N yr^{-1})		
Vegetation	3034	1,780[d] (2000s) 3,800[g] (1990s) 5,300[h] 2,940[i] (1990s)
Litter and soil	77161	106,000[d] (2000s) 100,000[g] (1990s) 56,800[h] 113,000[i] (1990s)
Ammonia	1924	163.7[d] (2000s) 361[h] 1200[i] (1990s)
Nitrate	2974	2,778[d] (2000s) 580[h] 14,800[i] (1990s)
N fluxes related to N cycling (Tg N yr^{-1})		
Plant uptake	940	618[d] (2000s) 1,127[g] (1990s) 1,084[h] 873[i] (1990s)
Net mineralization	947	
Mineralization	2045	1,678[d] (2000s)
Immobilization	1097	1,177[d] (2000s)
Nitrification	239	

https://doi.org/10.5194/bg-2020-147
Preprint. Discussion started: 14 May 2020

N losses (Tg N yr^{-1})			
NO_3- Leaching	53.5		97.1[b] (2001-2010) 62.8[d] (2000s) 77.0[g] (1990s)
NH_3 Volatilization	53.9		124.9[b] (2001-2010) 52.6[c] (early 1990s) 20.4[d] (2000s)
N_2 from denitrification	114.2		105.8[b] (2001-2010) 68[f] (year 2000)
N_2O from denitrification	4.2	12.6	8.7[b] (2001-2010) 10.9[c] (early 1990s) 13.0[a]
N_2O from nitrification	8.4		
NO from denitrification	11.4	34.3	24.8[c] (early 1990s) 26.8[g] (1990s)
NO from nitrification	22.9		

[a]Fowler et al. (2013), [b]Zaehle (2013), [c]Galloway et al. (2004), [d]von Bloh et al. (2018), [e]Galloway et al. (2013), [f]Bouwman et al. (2013), [g]Zaehle et al. (2010), [h]Xu-Ri and Prentice (2008), [i]Wania et al. (2012)

https://doi.org/10.5194/bg-2020-147
Preprint. Discussion started: 14 May 2020

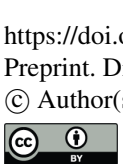

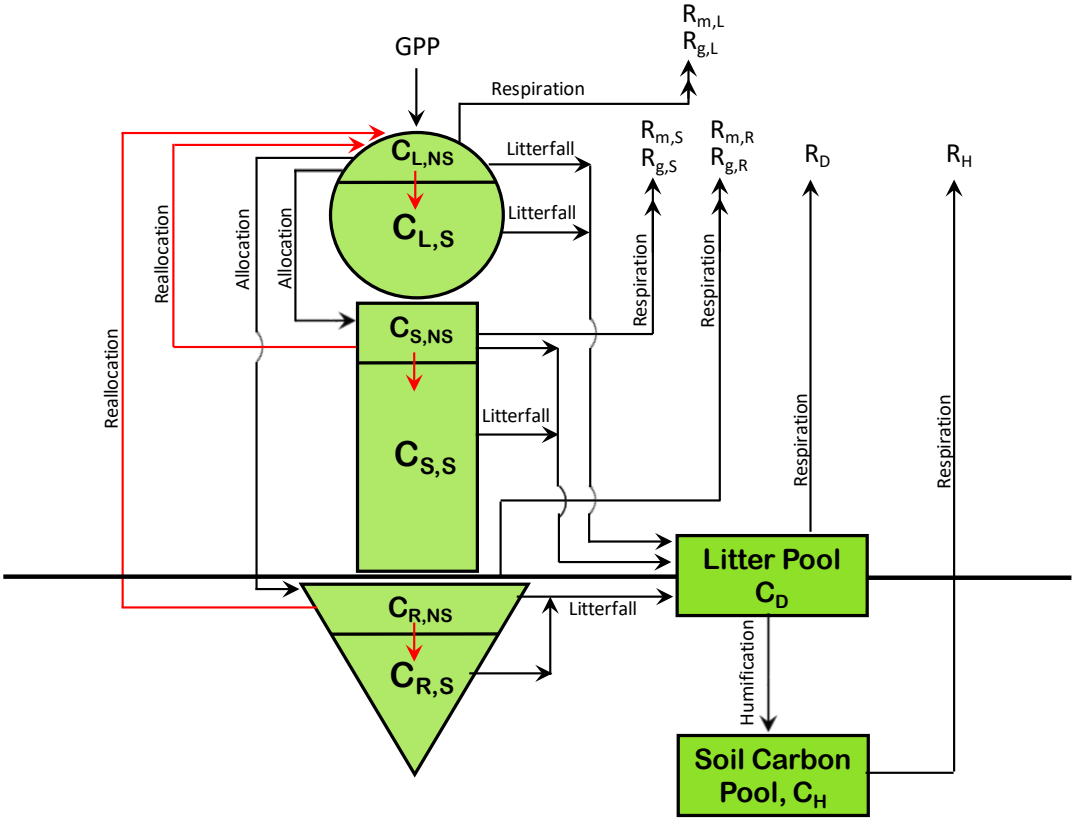

Figure 1: The structure of CLASSIC model used in this study, upon which the N cycle is implemented, with its carbon pools and fluxes. The fluxes of non-structural carbon are shown in red colour.

https://doi.org/10.5194/bg-2020-147
Preprint. Discussion started: 14 May 2020

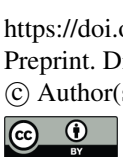

1304

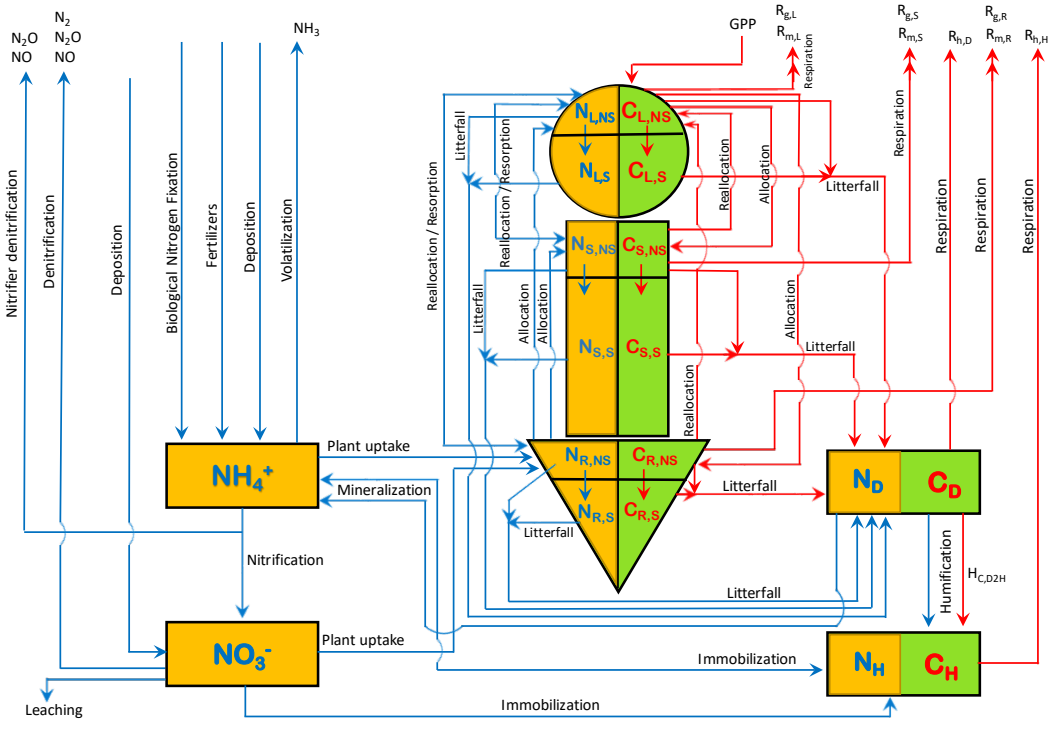

1305

1306 Figure 2: The structure of CLASSIC model used in this study. The eight prognostic carbon pools
1307 are shown in green colour and carbon fluxes in red colour. The ten prognostic nitrogen pools are
1308 shown in orange colour and nitrogen fluxes are shown in blue colour.

1309

1310

https://doi.org/10.5194/bg-2020-147
Preprint. Discussion started: 14 May 2020

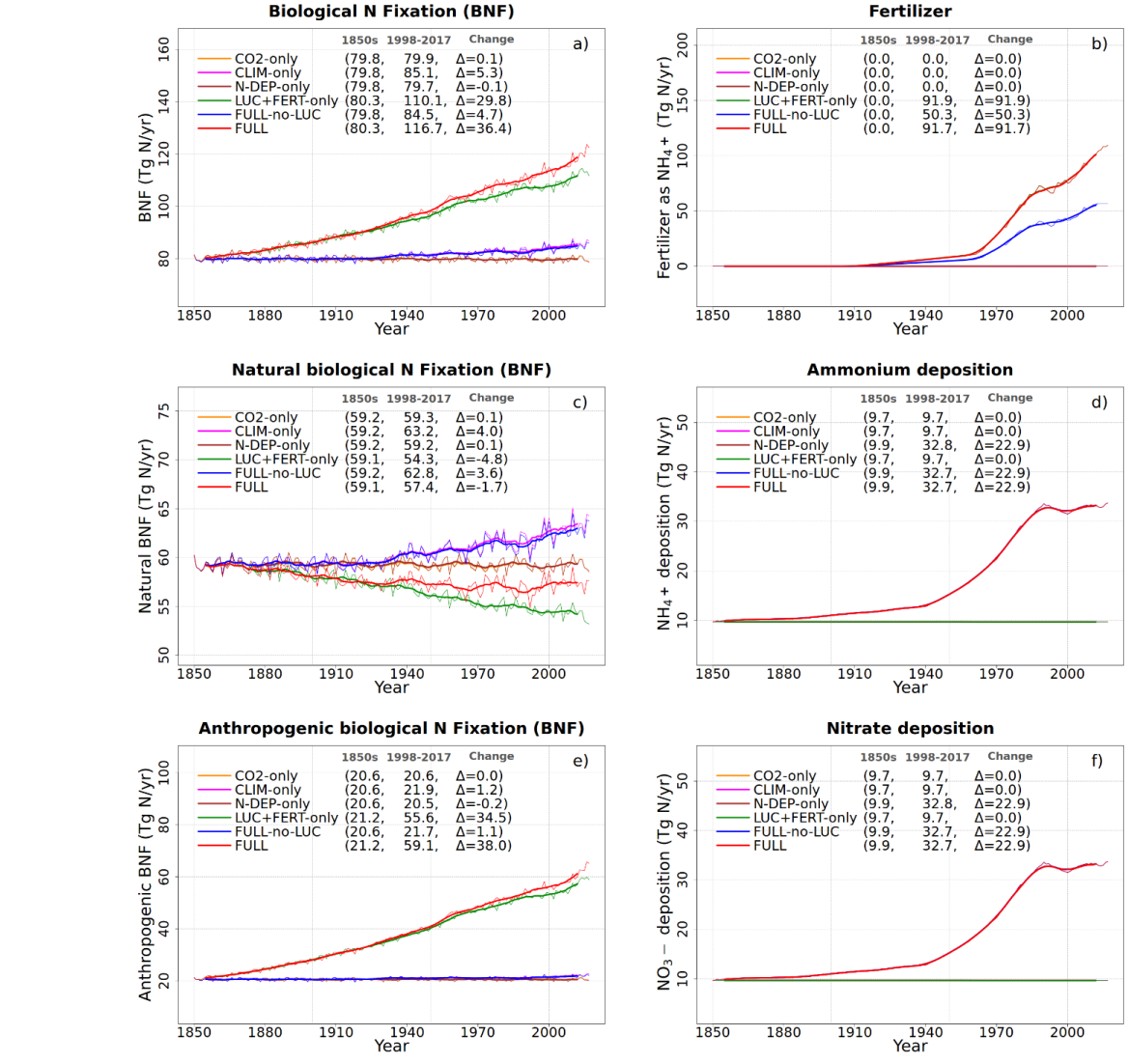

Figure 3: Global annual values of N inputs. Biological N fixation (a) and its break down into natural (c) and anthropogenic components (e). Fertilizer input (b) and atmospheric deposition of ammonium (d) and nitrate (f). The values in the parenthesis for legend entries show averages for the 1850s, the 1998-2017 period, and the change between 1850s and 1998-2017 periods. The thin lines show the annual values and the thick lines their 10-year moving average.

https://doi.org/10.5194/bg-2020-147
Preprint. Discussion started: 14 May 2020

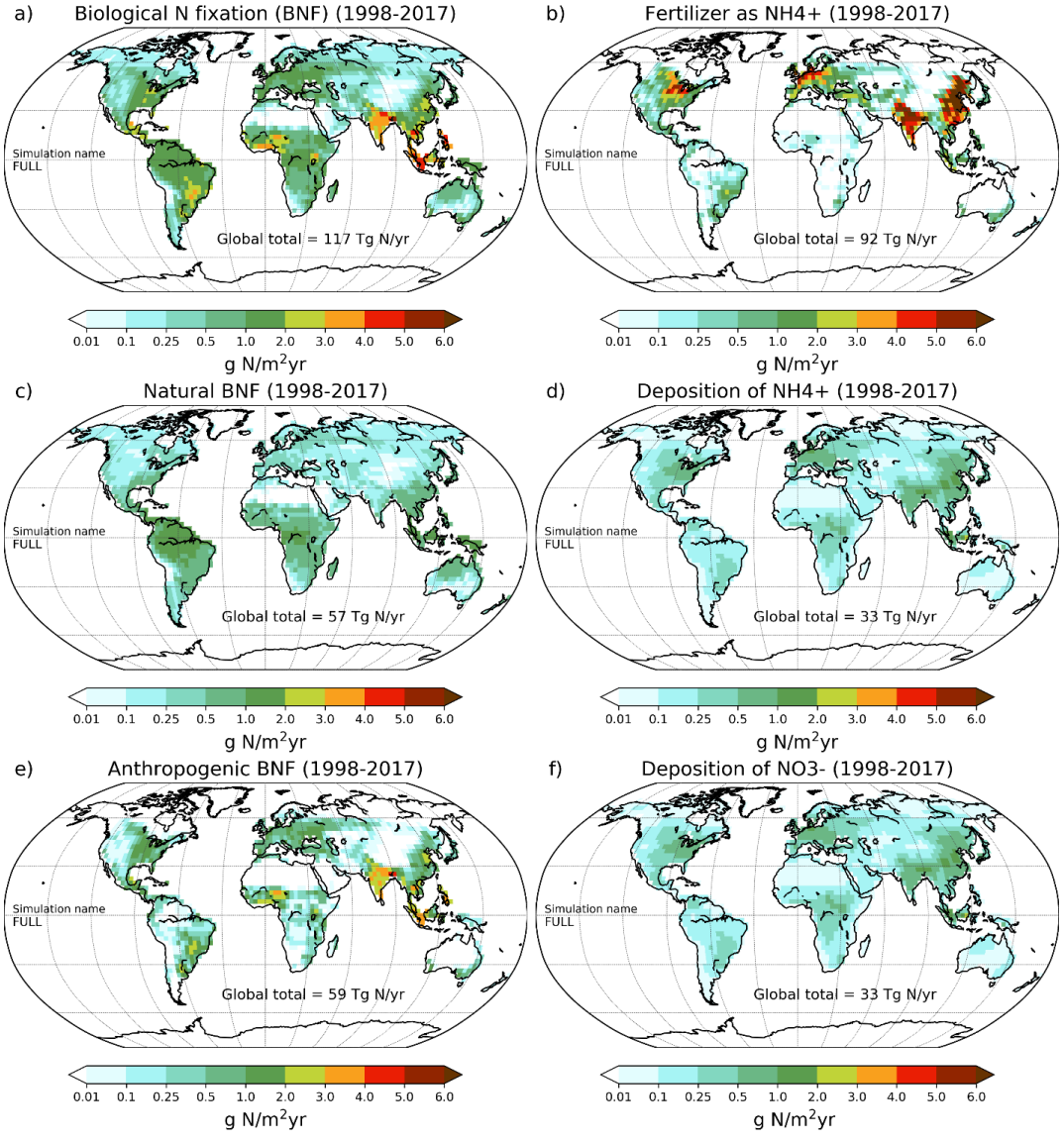

1317

1318 Figure 4: Geographical distribution of annual values of N inputs. Biological N fixation (a) and its
1319 break down into natural (c) and anthropogenic components (e). Fertilizer input (b) and
1320 atmospheric deposition of ammonium (d) and nitrate (f). The global total values shown are
1321 averaged over the 1998-2017 period. The thin lines show the annual values and the thick lines
1322 their 10-year moving average.

1323

https://doi.org/10.5194/bg-2020-147
Preprint. Discussion started: 14 May 2020

1324

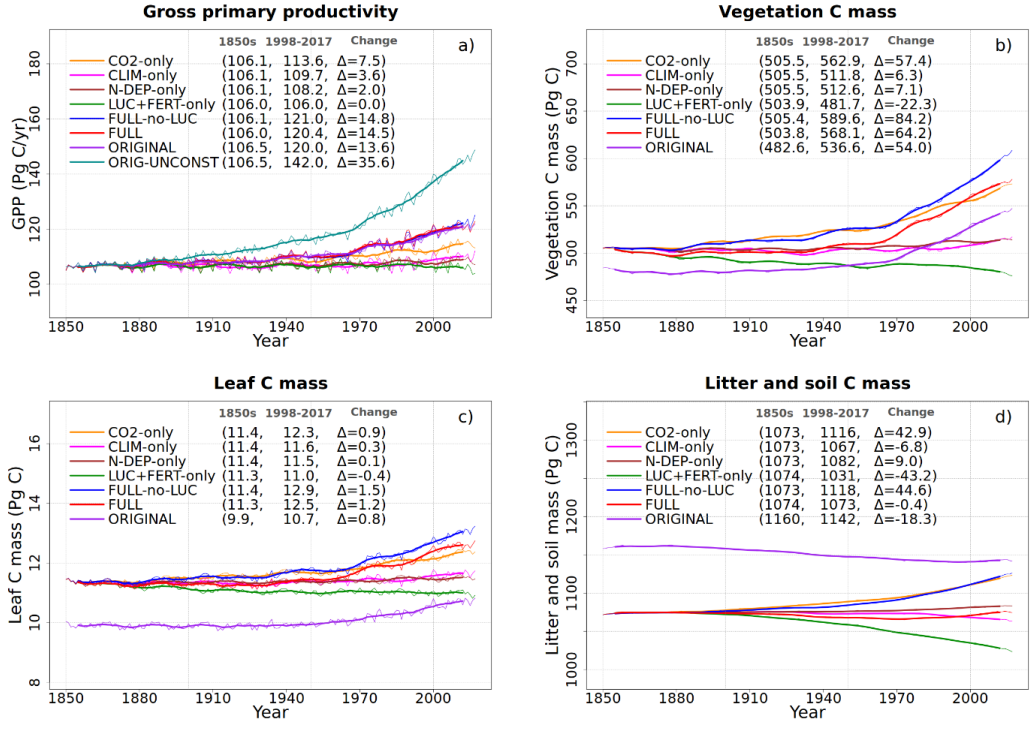

1325

1326 Figure 5: Global annual values of gross primary productivity (a), vegetation carbon (b), leaf
1327 carbon (c), and litter and soil carbon (d) for the primary simulations performed. The values in
1328 the parenthesis for legend entries show averages for the 1850s, the 1998-2017 period, and the
1329 change between 1850s and 1998-2017 periods. The thin lines show the annual values and the
1330 thick lines their 10-year moving average.

1331

https://doi.org/10.5194/bg-2020-147
Preprint. Discussion started: 14 May 2020

Biogeosciences Discussions
Open Access
EGU

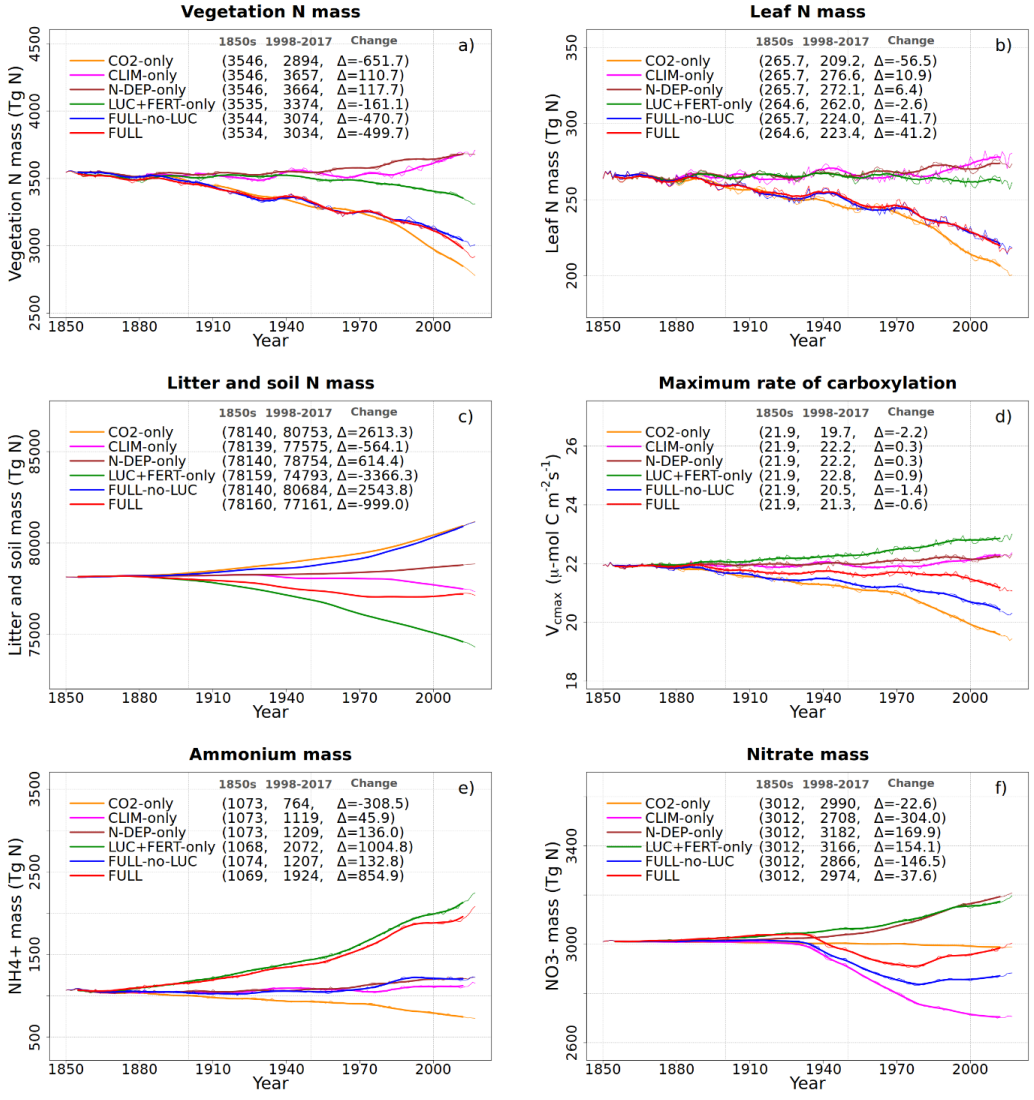

1332

1333 Figure 6: Global annual values of N in vegetation (a), leaves (b), litter and soil organic matter (c)
1334 pools, V_{cmax} (d), and ammonium (e), and nitrate (f) pools for the primary simulations performed.
1335 The values in the parenthesis for legend entries show averages for the 1850s, the 1998-2017
1336 period, and the change between 1850s and 1998-2017 periods. The thin lines show the annual
1337 values and the thick lines their 10-year moving average.

1338

https://doi.org/10.5194/bg-2020-147
Preprint. Discussion started: 14 May 2020

Biogeosciences
Discussions
Open Access
EGU

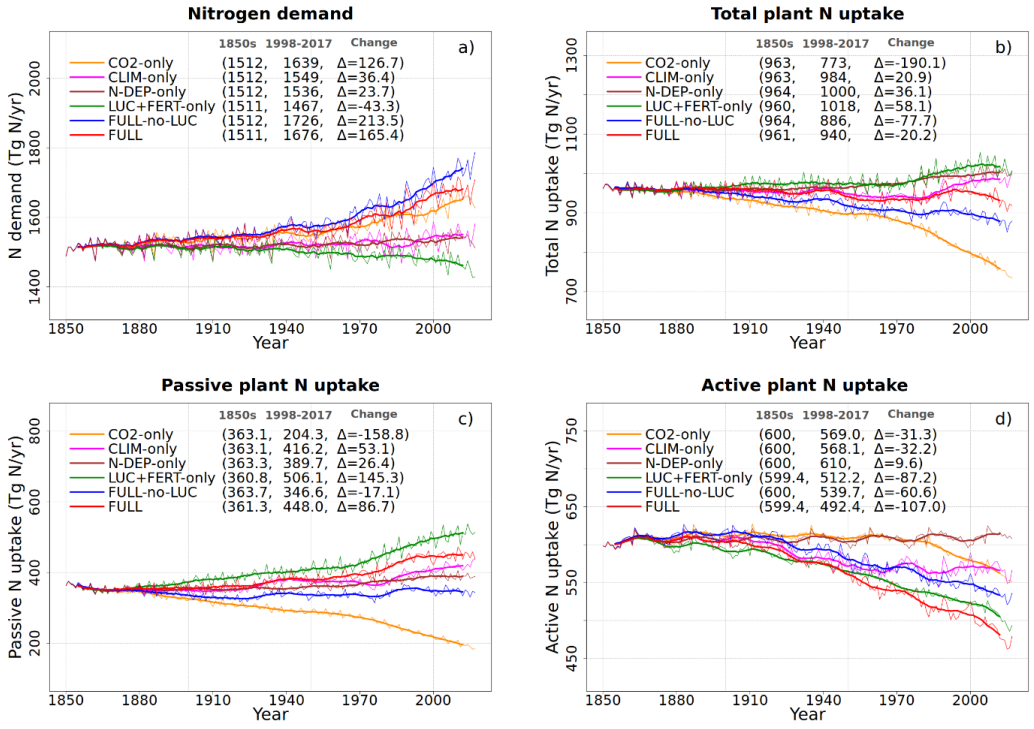

1339

1340

1341 Figure 7: Global annual values of N demand (a), total plant N uptake (b) and its split into passive
1342 (c) and active (d) components for the primary simulations performed. The values in the
1343 parenthesis for legend entries show averages for the 1850s, the 1998-2017 period, and the
1344 change between 1850s and 1998-2017 periods. The thin lines show the annual values and the
1345 thick lines their 10-year moving average.

1346

1347

https://doi.org/10.5194/bg-2020-147
Preprint. Discussion started: 14 May 2020

1348

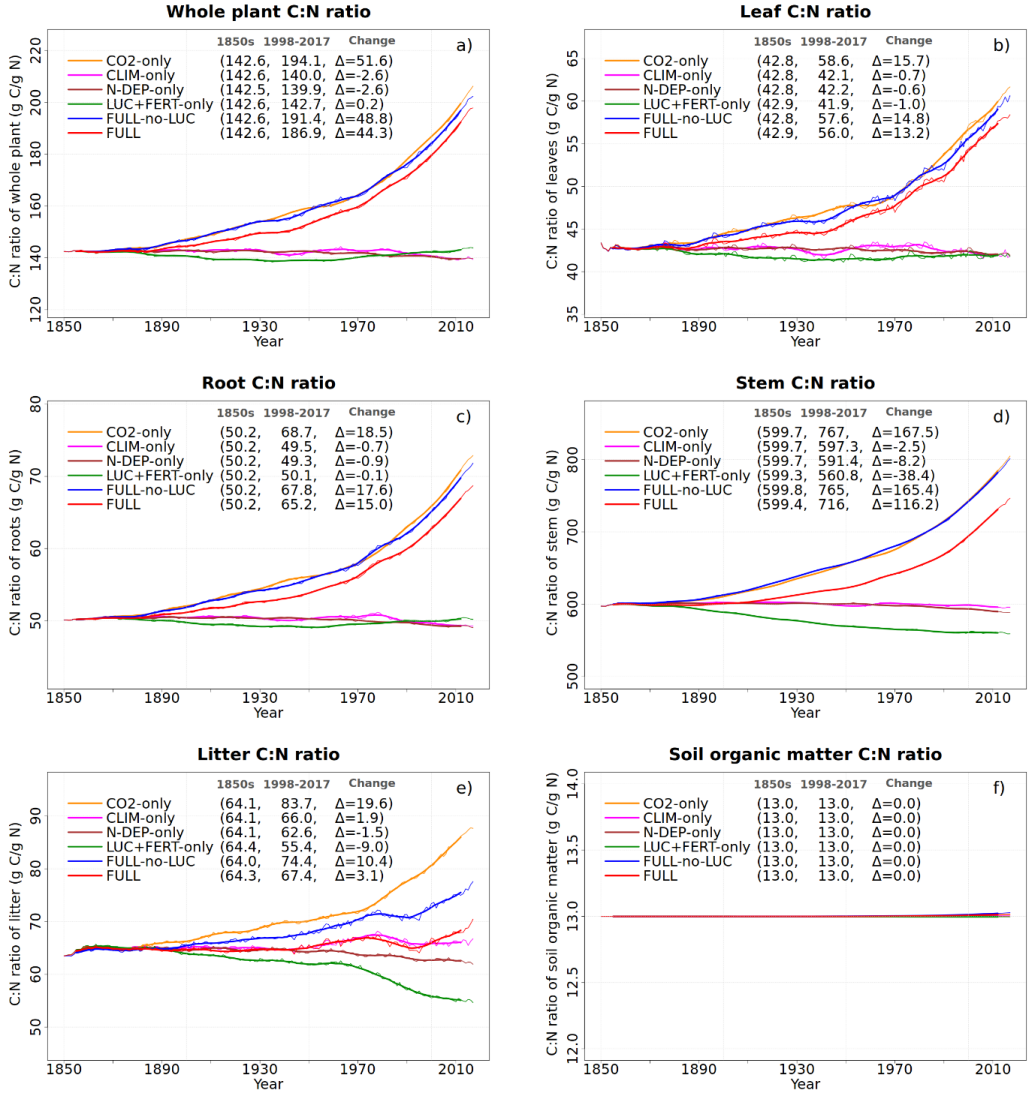

1349

1350 Figure 8: Global annual values of C:N ratios for whole plant (a), leaves (b) , root (c), stem (d),
1351 litter (e) and soil organic matter (f) pools from the primary six simulations. The values in the
1352 parenthesis for legend entries show averages for the 1850s, the 1998-2017 period, and the
1353 change between 1850s and 1998-2017 periods. The thin lines show the annual values and the
1354 thick lines their 10-year moving average.

1355

https://doi.org/10.5194/bg-2020-147
Preprint. Discussion started: 14 May 2020

1356

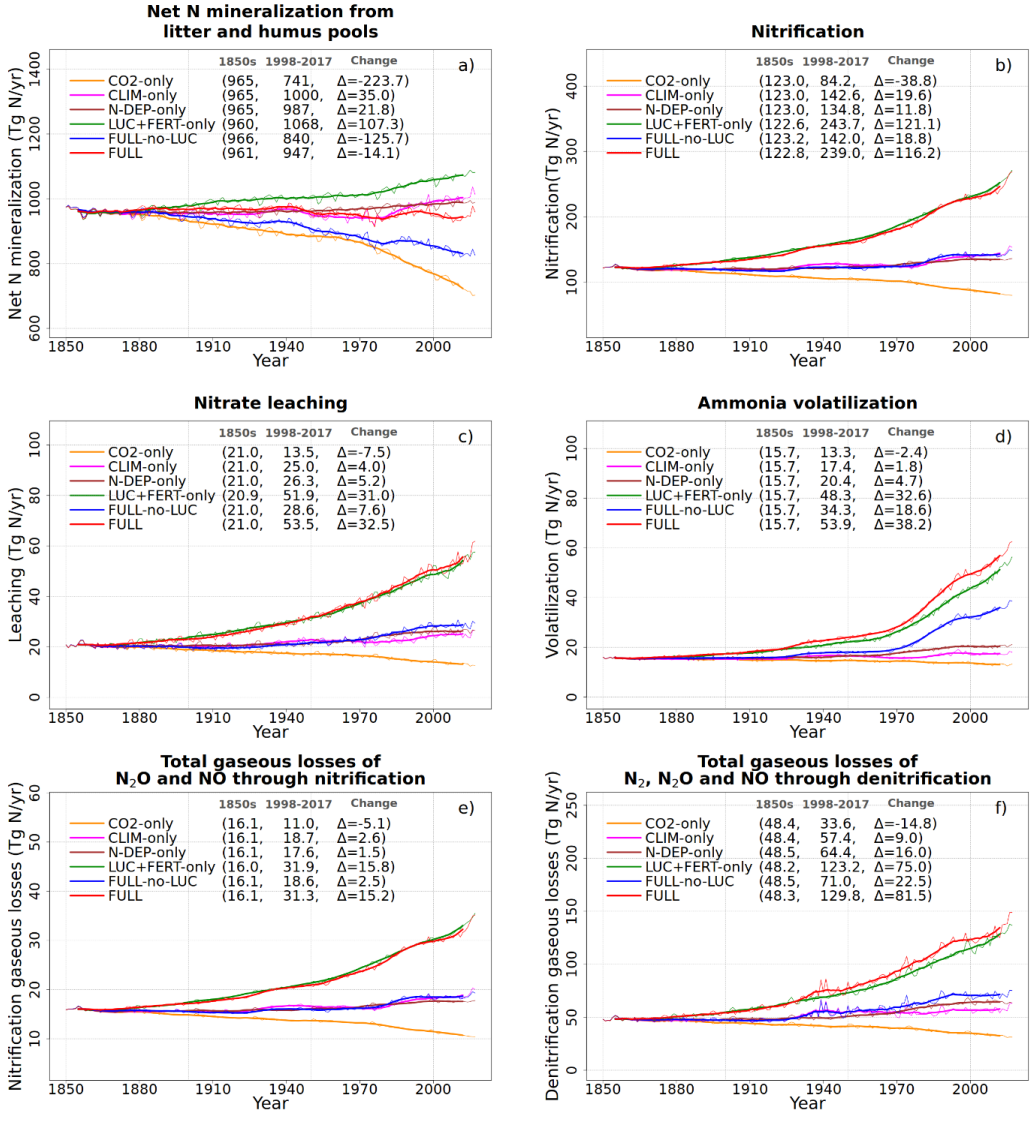

1357

1358 Figure 9: Global annual values of net mineralization (a), nitrification (b), NO_3- leaching (c), NH_3
1359 volatilization (d), and gaseous losses associated with nitrification (e) and denitrification (f) from
1360 the primary six simulations. The values in the parenthesis for legend entries show averages for
1361 the 1850s, the 1998-2017 period, and the change between 1850s and 1998-2017 periods. The
1362 thin lines show the annual values and the thick lines their 10-year moving average.

1363

https://doi.org/10.5194/bg-2020-147
Preprint. Discussion started: 14 May 2020

Biogeosciences
Discussions
Open Access
EGU

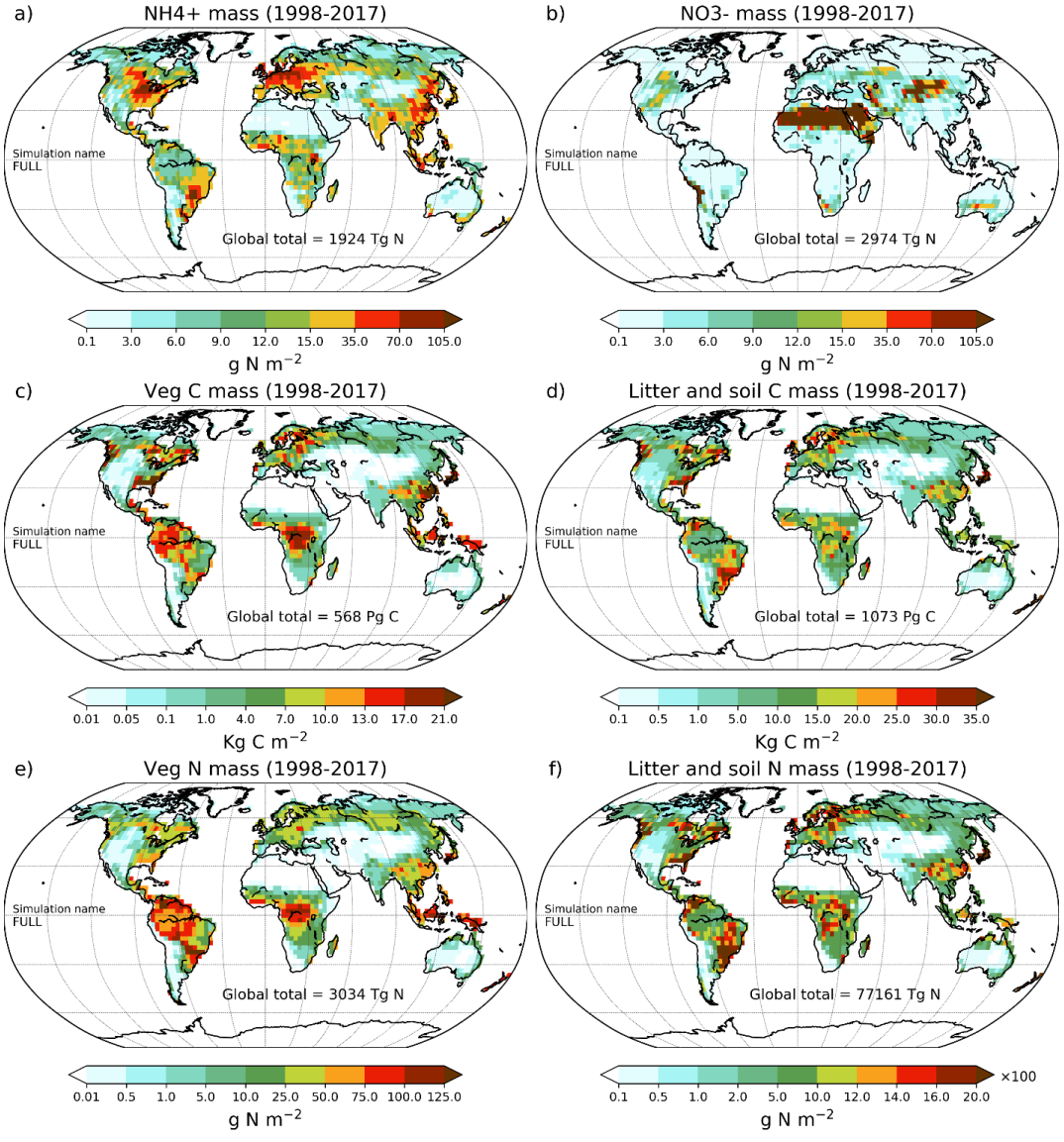

1364

1365 Figure 10: Geographical distribution of primary C and N pools. Ammonium (a), nitrate (b),
1366 vegetation C mass (c), litter and soil C mass (d), vegetation N mass (e), and litter and soil N mass
1367 (f). The global total values shown are averaged over the 1998-2017 period.

1368

https://doi.org/10.5194/bg-2020-147
Preprint. Discussion started: 14 May 2020

1369

1370

1371

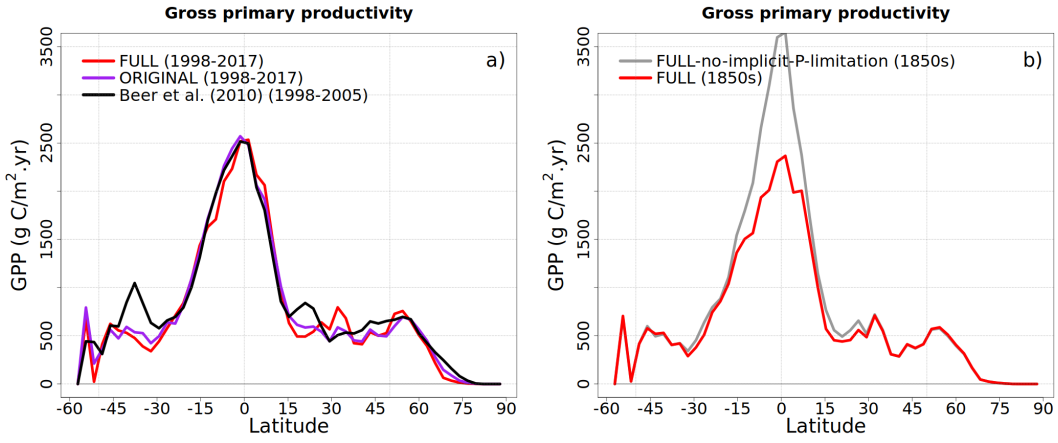

1372

1373 Figure 11: Comparison of zonal distribution of gross primary productivity (GPP). Panel (a)
1374 compares zonal distribution of GPP from FULL and ORIGINAL simulations with observation-
1375 based estimate from Beer at al. (2010) for the present day. Panel (b) compares the zonal
1376 distribution of GPP from the pre-industrial simulation, corresponding to 1850 conditions, from
1377 the FULL and FULL-no-implicit-P-limitation simulations to illustrate the effect of not reducing
1378 the Γ_1 parameter for calculating V_{cmax} for the broadleaf evergreen tree PFT that implicitly
1379 accounts for phosphorus limitation.

1380

1381

1382

https://doi.org/10.5194/bg-2020-147
Preprint. Discussion started: 14 May 2020

1383

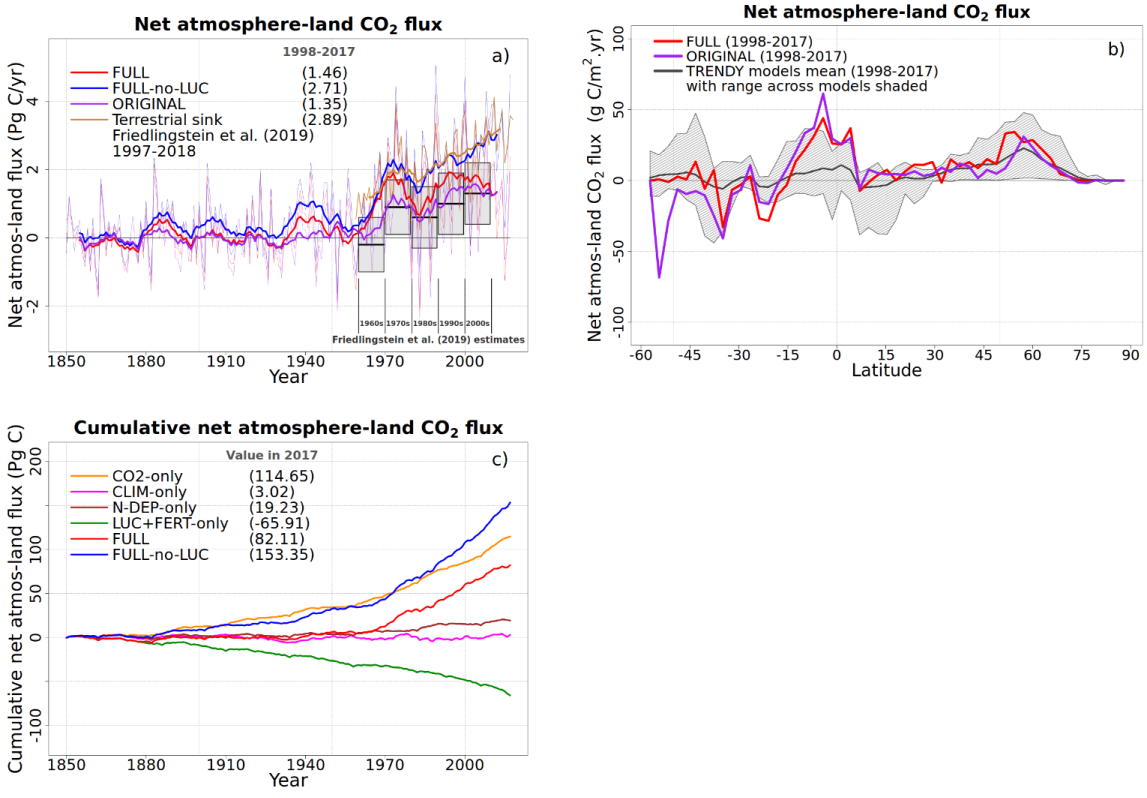

1384

1385 Figure 12: Comparison of simulated net atmosphere-land CO_2 flux from various simulations.
1386 Panel (a) compares globally-summed values of net atmosphere-land CO_2 flux from FULL, FULL-
1387 no-LUC simulation, and ORIGINAL simulations with estimate of terrestrial sink (dark yellow line)
1388 and net atmosphere-land CO2 flux (grey bars) from Friedlingstein et al. (2019). The thin lines
1389 show the annual values and the thick lines their 10-year moving average. Panel (b) compares
1390 zonal distribution of net atmosphere-land CO_2 flux from FULL and ORIGINAL simulations with
1391 the range from TRENDY models that contributed to the Friedlingstein et al. (2019) study. Panel
1392 (c) shows cumulative values of net atmosphere-land CO_2 flux from the six primary simulations
1393 to investigate the contribution of each forcing to the cumulative land carbon sink over the
1394 historical period.

1395

https://doi.org/10.5194/bg-2020-147
Preprint. Discussion started: 14 May 2020

References

Alexandrov, G. and Oikawa, T.: TsuBiMo: a biosphere model of the CO2-fertilization effect, Clim. Res., 19(3), 265–270, 2002.

Aragão, L. E. O. C., Malhi, Y., Metcalfe, D. B., Silva-Espejo, J. E., Jiménez, E., Navarrete, D., Almeida, S., Costa, A. C. L., Salinas, N., Phillips, O. L., Anderson, L. O., Alvarez, E., Baker, T. R., Goncalvez, P. H., Huamán-Ovalle, J., Mamani-Solórzano, M., Meir, P., Monteagudo, A., Patiño, S., Peñuela, M. C., Prieto, A., Quesada, C. A., Rozas-Dávila, A., Rudas, A., Silva Jr., J. A. and Vásquez, R.: Above- and below-ground net primary productivity across ten Amazonian forests on contrasting soils, Biogeosciences, 6(12), 2759–2778, doi:10.5194/bg-6-2759-2009, 2009.

Arneth, A., Harrison, S. P., Zaehle, S., Tsigaridis, K., Menon, S., Bartlein, P. J., Feichter, J., Korhola, A., Kulmala, M., O'Donnell, D., Schurgers, G., Sorvari, S. and Vesala, T.: Terrestrial biogeochemical feedbacks in the climate system, Nat. Geosci., 3(8), 525–532, doi:10.1038/ngeo905, 2010.

Arora, V. K.: Simulating energy and carbon fluxes over winter wheat using coupled land surface and terrestrial ecosystem models, Agric. For. Meteorol., 118(1), 21–47, doi:https://doi.org/10.1016/S0168-1923(03)00073-X, 2003.

Arora, V. K. and Boer, G. J.: A Representation of Variable Root Distribution in Dynamic Vegetation Models, Earth Interact., 7(6), 1–19, doi:10.1175/1087-3562(2003)007<0001:AROVRD>2.0.CO;2, 2003.

Arora, V. K. and Boer, G. J.: A parameterization of leaf phenology for the terrestrial ecosystem component of climate models, Glob. Change Biol., 11(1), 39–59, doi:10.1111/j.1365-2486.2004.00890.x, 2005.

Arora, V. K. and Boer, G. J.: Uncertainties in the 20th century carbon budget associated with land use change, Glob. Change Biol., 16(12), 3327–3348, doi:10.1111/j.1365-2486.2010.02202.x, 2010.

Arora, V. K. and Melton, J. R.: Reduction in global area burned and wildfire emissions since 1930s enhances carbon uptake by land, Nat. Commun., 9(1), 1326, doi:10.1038/s41467-018-03838-0, 2018.

Arora, V. K., Boer, G. J., Christian, J. R., Curry, C. L., Denman, K. L., Zahariev, K., Flato, G. M., Scinocca, J. F., Merryfield, W. J. and Lee, W. G.: The Effect of Terrestrial Photosynthesis Down Regulation on the Twentieth-Century Carbon Budget Simulated with the CCCma Earth System Model, J. Clim., 22(22), 6066–6088, doi:10.1175/2009JCLI3037.1, 2009.

Arora, V. K., Scinocca, J. F., Boer, G. J., Christian, J. R., Denman, K. L., Flato, G. M., Kharin, V. V., Lee, W. G. and Merryfield, W. J.: Carbon emission limits required to satisfy future representative concentration pathways of greenhouse gases, Geophys. Res. Lett., 38(5), doi:10.1029/2010GL046270, 2011.

Arora, V. K., Boer, G. J., Friedlingstein, P., Eby, M., Jones, C. D., Christian, J. R., Bonan, G., Bopp, L., Brovkin, V., Cadule, P., Hajima, T., Ilyina, T., Lindsay, K., Tjiputra, J. F. and Wu, T.: Carbon–Concentration and Carbon–Climate Feedbacks in CMIP5 Earth System Models, J. Clim., 26(15), 5289–5314, doi:10.1175/JCLI-D-12-00494.1, 2013.

Arora, V. K., Katavouta, A., Williams, R. G., Jones, C. D., Brovkin, V., Friedlingstein, P., Schwinger, J., Bopp, L., Boucher, O., Cadule, P., Chamberlain, M. A., Christian, J. R., Delire, C., Fisher, R. A., Hajima, T., Ilyina,

https://doi.org/10.5194/bg-2020-147
Preprint. Discussion started: 14 May 2020

1433 T., Joetzjer, E., Kawamiya, M., Koven, C., Krasting, J., Law, R. M., Lawrence, D. M., Lenton, A., Lindsay, K.,
1434 Pongratz, J., Raddatz, T., Séférian, R., Tachiiri, K., Tjiputra, J. F., Wiltshire, A., Wu, T. and Ziehn, T.:
1435 Carbon-concentration and carbon-climate feedbacks in CMIP6 models, and their comparison to CMIP5
1436 models, Biogeosciences Discuss., 2019, 1–124, doi:10.5194/bg-2019-473, 2019.

1437 Asaadi, A., Arora, V. K., Melton, J. R. and Bartlett, P.: An improved parameterization of leaf area index
1438 (LAI) seasonality in the Canadian Land Surface Scheme (CLASS) and Canadian Terrestrial Ecosystem
1439 Model (CTEM) modelling framework, Biogeosciences, 15(22), 6885–6907, doi:10.5194/bg-15-6885-2018,
1440 2018.

1441 Beer, C., Reichstein, M., Tomelleri, E., Ciais, P., Jung, M., Carvalhais, N., Rödenbeck, C., Arain, M. A.,
1442 Baldocchi, D., Bonan, G. B., Bondeau, A., Cescatti, A., Lasslop, G., Lindroth, A., Lomas, M., Luyssaert, S.,
1443 Margolis, H., Oleson, K. W., Roupsard, O., Veenendaal, E., Viovy, N., Williams, C., Woodward, F. I. and
1444 Papale, D.: Terrestrial Gross Carbon Dioxide Uptake: Global Distribution and Covariation with Climate,
1445 Science, 329(5993), 834–838, 2010.

1446 von Bloh, W., Schaphoff, S., Müller, C., Rolinski, S., Waha, K. and Zaehle, S.: Implementing the nitrogen
1447 cycle into the dynamic global vegetation, hydrology, and crop growth model LPJmL (version 5.0), Geosci.
1448 Model Dev., 11(7), 2789–2812, doi:10.5194/gmd-11-2789-2018, 2018.

1449 Bouwman, A. F., Beusen, A. H. W., Griffioen, J., Van Groenigen, J. W., Hefting, M. M., Oenema, O., Van
1450 Puijenbroek, P. J. T. M., Seitzinger, S., Slomp, C. P. and Stehfest, E.: Global trends and uncertainties in
1451 terrestrial denitrification and N2O emissions, Philos. Trans. R. Soc. B Biol. Sci., 368(1621), 20130112,
1452 doi:10.1098/rstb.2013.0112, 2013.

1453 Cao, M., Zhang, Q. and Shugart, H. H.: Dynamic responses of African ecosystem carbon cycling to climate
1454 change, Clim. Res., 17(2), 183–193, 2001.

1455 Clapp, R. B. and Hornberger, G. M.: Empirical equations for some soil hydraulic properties, Water
1456 Resour. Res., 14(4), 601–604, doi:10.1029/WR014i004p00601, 1978.

1457 Cleveland, C. C., Townsend, A. R., Schimel, D. S., Fisher, H., Howarth, R. W., Hedin, L. O., Perakis, S. S.,
1458 Latty, E. F., Von Fischer, J. C., Elseroad, A. and Wasson, M. F.: Global patterns of terrestrial biological
1459 nitrogen (N2) fixation in natural ecosystems, Glob. Biogeochem. Cycles, 13(2), 623–645,
1460 doi:10.1029/1999GB900014, 1999.

1461 Collatz, G., Ribas-Carbo, M. and Berry, J.: Coupled Photosynthesis-Stomatal Conductance Model for
1462 Leaves of C4 Plants, Funct. Plant Biol., 19(5), 519–538, 1992.

1463 Cotrufo, M. F., Ineson, P. and Scott, AndY.: Elevated CO2 reduces the nitrogen concentration of plant
1464 tissues, Glob. Change Biol., 4(1), 43–54, doi:10.1046/j.1365-2486.1998.00101.x, 1998.

1465 Croft, H., Chen, J. M., Luo, X., Bartlett, P., Chen, B. and Staebler, R. M.: Leaf chlorophyll content as a
1466 proxy for leaf photosynthetic capacity, Glob. Change Biol., 23(9), 3513–3524, doi:10.1111/gcb.13599,
1467 2017.

1468 Evans, J. R.: Photosynthesis and nitrogen relationships in leaves of C3 plants, Oecologia, 78(1), 9–19,
1469 doi:10.1007/BF00377192, 1989.

https://doi.org/10.5194/bg-2020-147
Preprint. Discussion started: 14 May 2020

1470 Eyring, V., Bony, S., Meehl, G. A., Senior, C. A., Stevens, B., Stouffer, R. J. and Taylor, K. E.: Overview of
1471 the Coupled Model Intercomparison Project Phase 6 (CMIP6) experimental design and organization,
1472 Geosci. Model Dev., 9(5), 1937–1958, doi:10.5194/gmd-9-1937-2016, 2016.

1473 Faria, T., Wilkins, D., Besford, R. T., Vaz, M., Pereira, J. S. and Chaves, M. M.: Growth at elevated CO2
1474 leads to down-regulation of photosynthesis and altered response to high temperature in Quercus suber
1475 L. seedlings, J. Exp. Bot., 47(11), 1755–1761, doi:10.1093/jxb/47.11.1755, 1996.

1476 Farquhar, G. D., von Caemmerer, S. and Berry, J. A.: A biochemical model of photosynthetic CO2
1477 assimilation in leaves of C3 species, Planta, 149(1), 78–90, doi:10.1007/BF00386231, 1980.

1478 Field, C. and Mooney, H.: The Photosynthesis-Nitrogen Relationship in Wild Plants, Biol. Int., 13, 25–56,
1479 1986.

1480 Fowler, D., Coyle, M., Skiba, U., Sutton, M. A., Cape, J. N., Reis, S., Sheppard, L. J., Jenkins, A., Grizzetti,
1481 B., Galloway, J. N., Vitousek, P., Leach, A., Bouwman, A. F., Butterbach-Bahl, K., Dentener, F., Stevenson,
1482 D., Amann, M. and Voss, M.: The global nitrogen cycle in the twenty-first century, Philos. Trans. R. Soc. B
1483 Biol. Sci., 368(1621), 20130164, doi:10.1098/rstb.2013.0164, 2013.

1484 Friedlingstein, P., Cox, P., Betts, R., Bopp, L., von Bloh, W., Brovkin, V., Cadule, P., Doney, S., Eby, M.,
1485 Fung, I., Bala, G., John, J., Jones, C., Joos, F., Kato, T., Kawamiya, M., Knorr, W., Lindsay, K., Matthews, H.
1486 D., Raddatz, T., Rayner, P., Reick, C., Roeckner, E., Schnitzler, K.-G., Schnur, R., Strassmann, K., Weaver,
1487 A. J., Yoshikawa, C. and Zeng, N.: Climate–Carbon Cycle Feedback Analysis: Results from the C4MIP
1488 Model Intercomparison, J. Clim., 19(14), 3337–3353, doi:10.1175/JCLI3800.1, 2006.

1489 Friedlingstein, P., Jones, M. W., O'Sullivan, M., Andrew, R. M., Hauck, J., Peters, G. P., Peters, W.,
1490 Pongratz, J., Sitch, S., Le Quéré, C., Bakker, D. C. E., Canadell, J. G., Ciais, P., Jackson, R. B., Anthoni, P.,
1491 Barbero, L., Bastos, A., Bastrikov, V., Becker, M., Bopp, L., Buitenhuis, E., Chandra, N., Chevallier, F.,
1492 Chini, L. P., Currie, K. I., Feely, R. A., Gehlen, M., Gilfillan, D., Gkritzalis, T., Goll, D. S., Gruber, N.,
1493 Gutekunst, S., Harris, I., Haverd, V., Houghton, R. A., Hurtt, G., Ilyina, T., Jain, A. K., Joetzjer, E., Kaplan, J.
1494 O., Kato, E., Klein Goldewijk, K., Korsbakken, J. I., Landschützer, P., Lauvset, S. K., Lefèvre, N., Lenton, A.,
1495 Lienert, S., Lombardozzi, D., Marland, G., McGuire, P. C., Melton, J. R., Metzl, N., Munro, D. R., Nabel, J.
1496 E. M. S., Nakaoka, S.-I., Neill, C., Omar, A. M., Ono, T., Peregon, A., Pierrot, D., Poulter, B., Rehder, G.,
1497 Resplandy, L., Robertson, E., Rödenbeck, C., Séférian, R., Schwinger, J., Smith, N., Tans, P. P., Tian, H.,
1498 Tilbrook, B., Tubiello, F. N., van der Werf, G. R., Wiltshire, A. J. and Zaehle, S.: Global Carbon Budget
1499 2019, Earth Syst. Sci. Data, 11(4), 1783–1838, doi:10.5194/essd-11-1783-2019, 2019.

1500 Galloway, J. N., Dentener, F. J., Capone, D. G., Boyer, E. W., Howarth, R. W., Seitzinger, S. P., Asner, G. P.,
1501 Cleveland, C. C., Green, P. A., Holland, E. A., Karl, D. M., Michaels, A. F., Porter, J. H., Townsend, A. R. and
1502 Vöosmarty, C. J.: Nitrogen Cycles: Past, Present, and Future, Biogeochemistry, 70(2), 153–226,
1503 doi:10.1007/s10533-004-0370-0, 2004.

1504 Galloway, J. N., Leach, A. M., Bleeker, A. and Erisman, J. W.: A chronology of human understanding of
1505 the nitrogen cycle†, Philos. Trans. R. Soc. B Biol. Sci., 368(1621), 20130120,
1506 doi:10.1098/rstb.2013.0120, 2013.

1507 Garnier, E., Salager, J.-L., Laurent, G. and Sonie, L.: Relationships between photosynthesis, nitrogen and
1508 leaf structure in 14 grass species and their dependence on the basis of expression, New Phytol., 143(1),
1509 119–129, doi:10.1046/j.1469-8137.1999.00426.x, 1999.

https://doi.org/10.5194/bg-2020-147
Preprint. Discussion started: 14 May 2020

1510 Gerber, S., Hedin, L. O., Oppenheimer, M., Pacala, S. W. and Shevliakova, E.: Nitrogen cycling and
1511 feedbacks in a global dynamic land model, Glob. Biogeochem. Cycles, 24(1),
1512 doi:10.1029/2008GB003336, 2010.

1513 Goll, D. S., Brovkin, V., Parida, B. R., Reick, C. H., Kattge, J., Reich, P. B., van Bodegom, P. M. and
1514 Niinemets, Ü.: Nutrient limitation reduces land carbon uptake in simulations with a model of combined
1515 carbon, nitrogen and phosphorus cycling, Biogeosciences, 9(9), 3547–3569, doi:10.5194/bg-9-3547-
1516 2012, 2012.

1517 Goyal, S. S. and Huffaker, R. C.: Nitrogen toxicity in plants, in Nitrogen in Crop Production, pp. 97–118,
1518 American Society of Agronomy, Madison, WI., 1984.

1519 Hungate, B. A., Dukes, J. S., Shaw, M. R., Luo, Y. and Field, C. B.: Nitrogen and Climate Change, Science,
1520 302(5650), 1512–1513, doi:10.1126/science.1091390, 2003.

1521 Hurtt, G. C., Frolking, S., Fearon, M. G., Moore, B., Shevliakova, E., Malyshev, S., Pacala, S. W. and
1522 Houghton, R. A.: The underpinnings of land-use history: three centuries of global gridded land-use
1523 transitions, wood-harvest activity, and resulting secondary lands, Glob. Change Biol., 12(7), 1208–1229,
1524 doi:10.1111/j.1365-2486.2006.01150.x, 2006.

1525 Jiang, M., Zaehle, S., De Kauwe, M. G., Walker, A. P., Caldararu, S., Ellsworth, D. S. and Medlyn, B. E.: The
1526 quasi-equilibrium framework revisited: analyzing long-term CO2 enrichment responses in plant–soil
1527 models, Geosci. Model Dev., 12(5), 2069–2089, doi:10.5194/gmd-12-2069-2019, 2019.

1528 Jones, A. G., Scullion, J., Ostle, N., Levy, P. E. and Gwynn-Jones, D.: Completing the FACE of elevated CO2
1529 research, Environ. Int., 73, 252–258, doi:https://doi.org/10.1016/j.envint.2014.07.021, 2014.

1530 Jones, C. D., Arora, V., Friedlingstein, P., Bopp, L., Brovkin, V., Dunne, J., Graven, H., Hoffman, F., Ilyina,
1531 T., John, J. G., Jung, M., Kawamiya, M., Koven, C., Pongratz, J., Raddatz, T., Randerson, J. T. and Zaehle,
1532 S.: C4MIP – The Coupled Climate–Carbon Cycle Model Intercomparison Project: experimental protocol
1533 for CMIP6, Geosci. Model Dev., 9(8), 2853–2880, doi:10.5194/gmd-9-2853-2016, 2016.

1534 Kattge, J., Knorr, W., Raddatz, T. and Wirth, C.: Quantifying photosynthetic capacity and its relationship
1535 to leaf nitrogen content for global-scale terrestrial biosphere models, Glob. Change Biol., 15(4), 976–
1536 991, doi:10.1111/j.1365-2486.2008.01744.x, 2009.

1537 Klein Goldewijk, K., Beusen, A., Doelman, J. and Stehfest, E.: Anthropogenic land use estimates for the
1538 Holocene – HYDE 3.2, Earth Syst. Sci. Data, 9(2), 927–953, doi:10.5194/essd-9-927-2017, 2017.

1539 Köchy, M., Hiederer, R. and Freibauer, A.: Global distribution of soil organic carbon – Part 1: Masses and
1540 frequency distributions of SOC stocks for the tropics, permafrost regions, wetlands, and the world, SOIL,
1541 1(1), 351–365, doi:10.5194/soil-1-351-2015, 2015.

1542 Kurz, W. A., Beukema, S. J. and Apps, M. J.: Estimation of root biomass and dynamics for the carbon
1543 budget model of the Canadian forest sector, Can. J. For. Res., 26(11), 1973–1979, doi:10.1139/x26-223,
1544 1996.

1545 Le Quéré, C., Andrew, R. M., Friedlingstein, P., Sitch, S., Hauck, J., Pongratz, J., Pickers, P. A., Korsbakken,
1546 J. I., Peters, G. P., Canadell, J. G., Arneth, A., Arora, V. K., Barbero, L., Bastos, A., Bopp, L., Chevallier, F.,

https://doi.org/10.5194/bg-2020-147
Preprint. Discussion started: 14 May 2020

1547 Chini, L. P., Ciais, P., Doney, S. C., Gkritzalis, T., Goll, D. S., Harris, I., Haverd, V., Hoffman, F. M.,
1548 Hoppema, M., Houghton, R. A., Hurtt, G., Ilyina, T., Jain, A. K., Johannessen, T., Jones, C. D., Kato, E.,
1549 Keeling, R. F., Goldewijk, K. K., Landschützer, P., Lefèvre, N., Lienert, S., Liu, Z., Lombardozzi, D., Metzl,
1550 N., Munro, D. R., Nabel, J. E. M. S., Nakaoka, S., Neill, C., Olsen, A., Ono, T., Patra, P., Peregon, A., Peters,
1551 W., Peylin, P., Pfeil, B., Pierrot, D., Poulter, B., Rehder, G., Resplandy, L., Robertson, E., Rocher, M.,
1552 Rödenbeck, C., Schuster, U., Schwinger, J., Séférian, R., Skjelvan, I., Steinhoff, T., Sutton, A., Tans, P. P.,
1553 Tian, H., Tilbrook, B., Tubiello, F. N., van der Laan-Luijkx, I. T., van der Werf, G. R., Viovy, N., Walker, A.
1554 P., Wiltshire, A. J., Wright, R., Zaehle, S. and Zheng, B.: Global Carbon Budget 2018, Earth Syst. Sci. Data,
1555 10(4), 2141–2194, doi:10.5194/essd-10-2141-2018, 2018.

1556 Leith, H.: Modeling the primary productivity of the world, in Primary Productivity of the Biosphere (H.
1557 Leith and R. H. Whittaker, Eds.), pp. 237–263, Springer-Verlag, Berlin and New York., 1975.

1558 Liang, J., Qi, X., Souza, L. and Luo, Y.: Processes regulating progressive nitrogen limitation under elevated
1559 carbon dioxide: a meta-analysis, Biogeosciences, 13(9), 2689–2699, doi:10.5194/bg-13-2689-2016, 2016.

1560 Manzoni, S., Jackson, R. B., Trofymow, J. A. and Porporato, A.: The Global Stoichiometry of Litter
1561 Nitrogen Mineralization, Science, 321(5889), 684–686, doi:10.1126/science.1159792, 2008.

1562 McGuire, A. D., Melillo, J. M. and Joyce, L. A.: THE ROLE OF NITROGEN IN THE RESPONSE OF FOREST NET
1563 PRIMARY PRODUCTION TO ELEVATED ATMOSPHERIC CARBON DIOXIDE, Annu. Rev. Ecol. Syst., 26(1),
1564 473–503, doi:10.1146/annurev.es.26.110195.002353, 1995.

1565 Melton, J. R. and Arora, V. K.: Competition between plant functional types in the Canadian Terrestrial
1566 Ecosystem Model (CTEM) v. 2.0, Geosci Model Dev, 9(1), 323–361, doi:10.5194/gmd-9-323-2016, 2016.

1567 Melton, J. R., Shrestha, R. K. and Arora, V. K.: The influence of soils on heterotrophic respiration exerts a
1568 strong control on net ecosystem productivity in seasonally dry Amazonian forests, Biogeosciences, 12(4),
1569 1151–1168, doi:10.5194/bg-12-1151-2015, 2015.

1570 Melton, J. R., Arora, V. K., Wisernig-Cojoc, E., Seiler, C., Fortier, M., Chan, E. and Teckentrup, L.: CLASSIC
1571 v1.0: the open-source community successor to the Canadian Land Surface Scheme (CLASS) and the
1572 Canadian Terrestrial Ecosystem Model (CTEM) – Part 1: Model framework and site-level performance,
1573 Geosci. Model Dev. Discuss., 2019, 1–40, doi:10.5194/gmd-2019-329, 2019.

1574 Ochoa-Hueso, R., Maestre, F. T., Ríos, A. [de los, Valea, S., Theobald, M. R., Vivanco, M. G., Manrique, E.
1575 and Bowker, M. A.: Nitrogen deposition alters nitrogen cycling and reduces soil carbon content in low-
1576 productivity semiarid Mediterranean ecosystems, Environ. Pollut., 179, 185–193,
1577 doi:https://doi.org/10.1016/j.envpol.2013.03.060, 2013.

1578 O'Hara, G. W.: The Role of Nitrogen Fixation in Crop Production, J. Crop Prod., 1(2), 115–138,
1579 doi:10.1300/J144v01n02_05, 1998.

1580 Porporato, A., D'Odorico, P., Laio, F. and Rodriguez-Iturbe, I.: Hydrologic controls on soil carbon and
1581 nitrogen cycles. I. Modeling scheme, Adv. Water Resour., 26(1), 45–58,
1582 doi:https://doi.org/10.1016/S0309-1708(02)00094-5, 2003.

1583 Reich, P. B., Hungate, B. A. and Luo, Y.: Carbon-Nitrogen Interactions in Terrestrial Ecosystems in
1584 Response to Rising Atmospheric Carbon Dioxide, Annu. Rev. Ecol. Evol. Syst., 37(1), 611–636,
1585 doi:10.1146/annurev.ecolsys.37.091305.110039, 2006a.

1586 Reich, P. B., Hobbie, S. E., Lee, T., Ellsworth, D. S., West, J. B., Tilman, D., Knops, J. M. H., Naeem, S. and
1587 Trost, J.: Nitrogen limitation constrains sustainability of ecosystem response to CO2, Nature, 440(7086),
1588 922–925, doi:10.1038/nature04486, 2006b.

1589 Riddick, S., Ward, D., Hess, P., Mahowald, N., Massad, R. and Holland, E.: Estimate of changes in
1590 agricultural terrestrial nitrogen pathways and ammonia emissions from 1850 to present in
1591 the\hack\newline Community Earth System Model, Biogeosciences, 13(11), 3397–3426, doi:10.5194/bg-
1592 13-3397-2016, 2016.

1593 Salvagiotti, F., Cassman, K. G., Specht, J. E., Walters, D. T., Weiss, A. and Dobermann, A.: Nitrogen
1594 uptake, fixation and response to fertilizer N in soybeans: A review, Field Crops Res., 108(1), 1–13,
1595 doi:https://doi.org/10.1016/j.fcr.2008.03.001, 2008.

1596 Sanz-Sáez, Á., Erice, G., Aranjuelo, I., Nogués, S., Irigoyen, J. J. and Sánchez-Díaz, M.: Photosynthetic
1597 down-regulation under elevated CO2 exposure can be prevented by nitrogen supply in nodulated alfalfa,
1598 J. Plant Physiol., 167(18), 1558–1565, doi:https://doi.org/10.1016/j.jplph.2010.06.015, 2010.

1599 Still, C. J., Berry, J. A., Collatz, G. J. and DeFries, R. S.: Global distribution of C3 and C4 vegetation: Carbon
1600 cycle implications, Glob. Biogeochem. Cycles, 17(1), 6–1, doi:10.1029/2001GB001807, 2003.

1601 Swart, N. C., Cole, J. N. S., Kharin, V. V., Lazare, M., Scinocca, J. F., Gillett, N. P., Anstey, J., Arora, V.,
1602 Christian, J. R., Hanna, S., Jiao, Y., Lee, W. G., Majaess, F., Saenko, O. A., Seiler, C., Seinen, C., Shao, A.,
1603 Sigmond, M., Solheim, L., von Salzen, K., Yang, D. and Winter, B.: The Canadian Earth System Model
1604 version 5 (CanESM5.0.3), Geosci. Model Dev., 12(11), 4823–4873, doi:10.5194/gmd-12-4823-2019,
1605 2019.

1606 Thom, A. S.: Momentum, mass and heat exchange of plant communities, in Vegetation and the
1607 atmosphere, Vol. 1, Principles, edited by Monteith, J. L., Academic Press, London., 1975.

1608 Thornton, P. E., Lamarque, J.-F., Rosenbloom, N. A. and Mahowald, N. M.: Influence of carbon-nitrogen
1609 cycle coupling on land model response to CO2 fertilization and climate variability, Glob. Biogeochem.
1610 Cycles, 21(4), doi:10.1029/2006GB002868, 2007.

1611 Tian, H., Yang, J., Lu, C., Xu, R., Canadell, J. G., Jackson, R. B., Arneth, A., Chang, J., Chen, G., Ciais, P.,
1612 Gerber, S., Ito, A., Huang, Y., Joos, F., Lienert, S., Messina, P., Olin, S., Pan, S., Peng, C., Saikawa, E.,
1613 Thompson, R. L., Vuichard, N., Winiwarter, W., Zaehle, S., Zhang, B., Zhang, K. and Zhu, Q.: The Global
1614 N2O Model Intercomparison Project, Bull. Am. Meteorol. Soc., 99(6), 1231–1251, doi:10.1175/BAMS-D-
1615 17-0212.1, 2018.

1616 Tipping, E., Somerville, C. J. and Luster, J.: The C:N:P:S stoichiometry of soil organic matter,
1617 Biogeochemistry, 130(1), 117–131, doi:10.1007/s10533-016-0247-z, 2016.

1618 Tomasek, A., Kozarek, J. L., Hondzo, M., Lurndahl, N., Sadowsky, M. J., Wang, P. and Staley, C.:
1619 Environmental drivers of denitrification rates and denitrifying gene abundances in channels and riparian
1620 areas, Water Resour. Res., 53(8), 6523–6538, doi:10.1002/2016WR019566, 2017.

1621 Verseghy, D. L.: Class—A Canadian land surface scheme for GCMS. I. Soil model, Int. J. Climatol., 11(2),
1622 111–133, doi:10.1002/joc.3370110202, 1991.

1623 Verseghy, D. L., McFarlane, N. A. and Lazare, M.: Class—A Canadian land surface scheme for GCMS, II.
1624 Vegetation model and coupled runs, Int. J. Climatol., 13(4), 347–370, doi:10.1002/joc.3370130402,
1625 1993.

1626 Vitousek, P. M.: Litterfall, Nutrient Cycling, and Nutrient Limitation in Tropical Forests, Ecology, 65(1),
1627 285–298, doi:10.2307/1939481, 1984.

1628 Vitousek, P. M.: Beyond Global Warming: Ecology and Global Change, Ecology, 75(7), 1861–1876,
1629 doi:10.2307/1941591, 1994.

1630 Vitousek, P. M. and Howarth, R. W.: Nitrogen limitation on land and in the sea: How can it occur?,
1631 Biogeochemistry, 13(2), 87–115, doi:10.1007/BF00002772, 1991.

1632 Vitousek, P. M., Porder, S., Houlton, B. Z. and Chadwick, O. A.: Terrestrial phosphorus limitation:
1633 mechanisms, implications, and nitrogen–phosphorus interactions, Ecol. Appl., 20(1), 5–15,
1634 doi:10.1890/08-0127.1, 2010.

1635 Vitousek, P. M., Menge, D. N. L., Reed, S. C. and Cleveland, C. C.: Biological nitrogen fixation: rates,
1636 patterns and ecological controls in terrestrial ecosystems, Philos. Trans. R. Soc. B Biol. Sci., 368(1621),
1637 20130119, doi:10.1098/rstb.2013.0119, 2013.

1638 Wang, J., Liu, X., Zhang, X., Li, L., Lam, S. K. and Pan, G.: Changes in plant C, N and P ratios under elevated
1639 [CO2] and canopy warming in a rice-winter wheat rotation system, Sci. Rep., 9(1), 5424,
1640 doi:10.1038/s41598-019-41944-1, 2019.

1641 Wania, R., Meissner, K. J., Eby, M., Arora, V. K., Ross, I. and Weaver, A. J.: Carbon-nitrogen feedbacks in
1642 the UVic ESCM, Geosci. Model Dev., 5(5), 1137–1160, doi:10.5194/gmd-5-1137-2012, 2012.

1643 Wei, X., Shao, M., Gale, W. and Li, L.: Global pattern of soil carbon losses due to the conversion of
1644 forests to agricultural land, Sci. Rep., 4, 4062, 2014.

1645 Xu-Ri and Prentice, I. C.: Terrestrial nitrogen cycle simulation with a dynamic global vegetation model,
1646 Glob. Change Biol., 14(8), 1745–1764, doi:10.1111/j.1365-2486.2008.01625.x, 2008.

1647 Zaehle, S.: Terrestrial nitrogen and carbon cycle interactions at the global scale, Philos. Trans. R. Soc. B
1648 Biol. Sci., 368(1621), 20130125, doi:10.1098/rstb.2013.0125, 2013.

1649 Zaehle, S., Friend, A. D., Friedlingstein, P., Dentener, F., Peylin, P. and Schulz, M.: Carbon and nitrogen
1650 cycle dynamics in the O-CN land surface model: 2. Role of the nitrogen cycle in the historical terrestrial
1651 carbon balance: NITROGEN EFFECTS ON GLOBAL C CYCLING, Glob. Biogeochem. Cycles, 24(1), n/a-n/a,
1652 doi:10.1029/2009GB003522, 2010.

1653 Zeng, H., Jia, G. and Epstein, H.: Recent changes in phenology over the northern high latitudes detected
1654 from multi-satellite data, Environ. Res. Lett., 6(4), 045508, 2011.

https://doi.org/10.5194/bg-2020-147
Preprint. Discussion started: 14 May 2020

1655 Zhang, H., Goll, D. S., Manzoni, S., Ciais, P., Guenet, B. and Huang, Y.: Modeling the effects of litter
1656 stoichiometry and soil mineral N availability on soil organic matter formation using CENTURY-CUE (v1.0),
1657 Geosci. Model Dev., 11(12), 4779–4796, doi:10.5194/gmd-11-4779-2018, 2018.

1658 Zhao, X., Yang, Y., Shen, H., Geng, X. and Fang, J.: Global soil–climate–biome diagram: linking surface soil
1659 properties to climate and biota, Biogeosciences, 16(14), 2857–2871, doi:10.5194/bg-16-2857-2019,
1660 2019.

1661 Zhu, Z., Piao, S., Myneni, R. B., Huang, M., Zeng, Z., Canadell, J. G., Ciais, P., Sitch, S., Friedlingstein, P.,
1662 Arneth, A., Cao, C., Cheng, L., Kato, E., Koven, C., Li, Y., Lian, X., Liu, Y., Liu, R., Mao, J., Pan, Y., Peng, S.,
1663 Penuelas, J., Poulter, B., Pugh, T. A. M., Stocker, B. D., Viovy, N., Wang, X., Wang, Y., Xiao, Z., Yang, H.,
1664 Zaehle, S. and Zeng, N.: Greening of the Earth and its drivers, Nat. Clim Change, 6(8), 791–795, 2016.

1665 Zinke, P. J., Stangenberger, A. G., Post, W. M., Emanuel, W. R. and Olson, J. S.: Global Organic Soil
1666 Carbon and Nitrogen, Tech. Rep. ORNL/TM-8857, Oak Ridge National Laboratory, Oak Ridge, Tennessee,
1667 USA. [online] Available from: https://doi.org/10.3334/ORNLDAAC/221, 1998.

1668

1669

1670